

LONG WAVES GENERATION BY ATMOSPHERIC PRESSURE  
DISTURBANCES AND CASE STUDY

A THESIS SUBMITTED TO  
THE GRADUATE SCHOOL OF NATURAL AND APPLIED SCIENCES  
OF  
MIDDLE EAST TECHNICAL UNIVERSITY

BY

ÖZGE ÇABUK

IN PARTIAL FULFILLMENT OF THE REQUIREMENTS  
FOR  
THE DEGREE OF MASTER OF SCIENCE  
IN  
CIVIL ENGINEERING

AUGUST 2019



Approval of the thesis:

**LONG WAVES GENERATION BY ATMOSPHERIC PRESSURE  
DISTURBANCES AND CASE STUDY**

submitted by **ÖZGE ÇABUK** in partial fulfillment of the requirements for the degree  
of **MASTER OF SCIENCE in CIVIL ENGINEERING Department, Middle East  
Technical University** by,

Prof. Dr. Halil Kalıpçılar  
Dean, Graduate School of **Natural and Applied Sciences**

\_\_\_\_\_

Prof. Dr. Ahmet Türer  
Head of Department, **Civil Engineering**

\_\_\_\_\_

Prof. Dr. Ahmet Cevdet Yalçiner  
Supervisor, **Civil Engineering, METU**

\_\_\_\_\_

Assist. Prof. Dr. Gülizar Özyurt Tarakcıođlu  
Co-Supervisor, **Civil Engineering Department, METU**

\_\_\_\_\_

**Examining Committee Members:**

Prof. Dr. İsmail Yücel  
Civil Engineering Dept., METU

\_\_\_\_\_

Prof. Dr. Ahmet Cevdet Yalçiner  
Civil Engineering, METU

\_\_\_\_\_

Assist. Prof. Dr. Gülizar Özyurt Tarakcıođlu  
Civil Engineering Dept., METU

\_\_\_\_\_

Assoc. Prof. Dr. Yakup Darama  
Civil Engineering Dept., Atılım University

\_\_\_\_\_

Assist. Prof. Dr. Cüneyt Baykal  
Civil Engineering Dept., METU

\_\_\_\_\_

Date: 05.08.2019

**I hereby declare that all information in this document has been obtained and presented in accordance with academic rules and ethical conduct. I also declare that, as required by these rules and conduct, I have fully cited and referenced all material and results that are not original to this work.**

Name, Surname: Özge Çabuk

Signature:

## ABSTRACT

### LONG WAVES GENERATION BY ATMOSPHERIC PRESSURE DISTURBANCES AND CASE STUDY

Çabuk, Özge  
MASTER OF SCIENCE, CIVIL ENGINEERING  
Supervisor: Prof. Dr. Ahmet Cevdet Yalçın  
Co-Supervisor: Assist. Prof. Dr. Gülizar Özyurt Tarakcıoğlu

August 2019, 76 pages

One of the interesting marine events is the long wave generation due to spatial and temporal changes of atmospheric pressure and wind fields during storm events. These kind of phenomena is called as storm surge and cause basin wide and local water level changes in sea surface and sometimes amplifies at some regions. There are examples of these kinds of event in all over the world. In this study the atmospheric pressure and wind fields are used as the input to the numerical model NAMI DANCE which solves Nonlinear Shallow Water Equations. The new modified version of the numerical model is tested using regular shaped pressure and wind fields in regular shaped flat basins. It is applied to case studies in Caribbean region for Irma and Maria Hurricanes and the results are compared with the observations. The model is also applied to recently happened January 18, 2018 Aegean Sea Storm Event and September 29-30 18, 2018 Medicane Event.

Keywords: Storm surge, atmospheric pressure disturbances, long waves, numerical modeling

## ÖZ

### ATMOSFERİK BASINÇ DEĞİŞİMLERİNE GÖRE UZUN PERİYOTLU DALGALAR VE OLAY İNCELEMESİ

Çabuk, Özge  
Yüksek Lisans, İnşaat Mühendisliği  
Tez Danışmanı: Prof. Dr. Ahmet Cevdet Yalçiner  
Ortak Tez Danışmanı: Dr. Öğr. Üyesi Gülizar Özyurt Tarakcıoğlu

Ağustos 2019, 76 sayfa

Denizlerde rastlanan ilginç olaylardan birisi de fırtına sırasında atmosferik basınç ve rüzgar alanlarının mekansal ve zamansal değişimlerinden oluşan uzun dönemli dalgalardır. Fırtına kabarması olarak adlandırılan bu olaylar, geniş bir alanda ya da yerel bir bölgede su seviyesi değişimine sebep olup bölge özelliklerine göre bazı alanlarda daha fazla su yükselmesine neden olabilir. Bu olaylara dünyanın birçok yerinde rastlanabilmektedir. Bu çalışmada zamansal ve alansal atmosferik basınç değişimlerini kapsayan veriler, doğrusal olmayan sıvı su denklemlerini çözen NAMI DANCE sayısal modeline girdi olarak verilmiştir. Sayısal modelin değiştirilmiş versiyonu, düz havzalarda, düzenli basınç ve rüzgar alanları kullanılarak test edilmiştir. Daha sonra, sayısal model, Karayipler Bölgesi'ndeki Irma ve Maria Kasırgaları için test edilmiş ve sonuçlar gözlemlerle karşılaştırılmıştır. Ayrıca, bu model, yakın zamanda meydana gelen 18 Ocak 2018 Ege Denizi Fırtına olayı ve 29-30 Eylül 2018 Medicane olayı vakalarına da uygulanmıştır.

Anahtar Kelimeler: Fırtına kabarması, atmosferik basınç değişimleri, uzun periyotlu dalgalarda, sayısal modelleme

<to my beloved family>

## ACKNOWLEDGEMENTS

I would like to thank the people who have supported me during my studies, contribute to my education and leading me in the right direction.

First of all, I would like to express my gratitude to *Prof. Dr. Ahmet Cevdet Yalçiner* for his significant support, contribution and giving me motivation during my studies and his patience.

I am very grateful to *Dr. Işıkhan Güler* for his contributions, support, understanding and high-spirited personality.

I am particularly thankful to *Prof. Dr. Ayşen Ergin* for her love, guidance and endless support. It is always a pleasure to work with her.

I would like to thank *Assist. Prof. Dr. Gülizar Özyurt Tarakcıoğlu* for her contribution to my study and guidance.

I am also thankful to *Assist. Prof. Dr. Cüneyt Baykal* for his contribution to my coastal and ocean engineering education.

Special thanks to *Bora Yalçiner* for his valuable contributions to my research.

I am grateful to the faculty staff of Coastal and Ocean Engineering of the Middle East Technical University for support and help.

Last but not least, I am very thankful to my dear family for their endless support, patience and love in every step of my life and my friends for giving me courage and motivation.

## TABLE OF CONTENTS

ABSTRACT .....	v
ÖZ .....	vi
ACKNOWLEDGEMENTS .....	viii
TABLE OF CONTENTS .....	ix
LIST OF TABLES .....	xi
LIST OF FIGURES .....	xii
CHAPTERS	
1. INTRODUCTION .....	1
2. LITERATURE SURVEY .....	5
2.1. Long Waves Generated by Atmospheric Pressure Forcing.....	5
2.2. The Surface Wind Drag Coefficient.....	10
2.3. Storm Surge Modeling .....	12
3. STORM SURGE MODELING .....	15
3.1. NAMI DANCE Tsunami Model .....	15
3.2. Storm Surge Modeling with NAMI DANCE.....	18
4. VALIDATION AND VERIFICATION OF NUMERICAL MODEL.....	27
4.1. Verification and Validation Procedures in Modeling.....	27
4.2. Verification by Static Pressure Conditions in Regular Shaped Basin.....	28
4.2.1. Verification by Static Circular Low Pressure Condition (Cyclone Condition).....	28

4.2.2. Verification by Static Circular High Pressure Condition (Anticyclone Condition).....	30
4.3. Application to Case Studies .....	32
4.3.1. Application to 30 August–12 September, 2017 Cyclone Irma event.....	32
4.3.2. Application to September 16-30, 2017 Cyclone Maria event .....	42
4.3.3. Application to 16-25 January, 2018 Aegean Event.....	53
4.3.4. Application to September 29-October 01, 2018 Medicane Event.....	57
5. CONCLUSION .....	63
Future Recommendations: .....	65
REFERENCES .....	67
APPENDIX.....	73

## LIST OF TABLES

### TABLES

Table 3.1. Wave Components effective in storm surge (Ergin,2010).....	19
Table 4.1. The surface observations from selected land stations, National Hurricane Center, Hurricane Irma Report, 2017.....	36
Table 4.2. Detailed information about selected domains.....	37
Table 4.3. The comparison of the simulation results and observed values for Antigua, Barbuda and Vieques Islands .....	40
Table 4.4. The maximum water levels and their arrival time for GDL-2, GDL-1, MRG, PTM and MTQ.....	49
Table 4.5. The detailed information about size of bathymetry .....	54
Table 4.6. The calculated maximum water level and their arrival time for selected locations Izmir and Bodrum.....	55
Table 4.7. The information of the model domain .....	58
Table 4.8. The calculated max.and min. water level change and arrival time of max. water level for Stazzo, Nea Kios and Akyaka.....	59

## LIST OF FIGURES

### FIGURES

Figure 1.1. Tropical cyclone events around the world, (NOAA, Historical Hurricane Tracks data base) .....	2
Figure 3.1. Modeling process of NAMI DANCE (Velioglu, 2017).....	17
Figure 3.2. A diagram of various physical processes (Alymov,2005). .....	21
Figure 3.3. The variables of the shallow water model and their coordinates (Probst and Franchello, 2012).....	23
Figure 4.1. The model verification and validation process (Schlesinger,1979).....	27
Figure 4.2. Bathymetry with low pressure at the center .....	28
Figure 4.3. Water elevation change at the center due to low pressure .....	29
Figure 4.4. Bathymetry with high pressure at the center .....	30
Figure 4.5. Water elevation change at the center due to high pressure .....	31
Figure 4.6. The path of the Hurricane Irma, 30 August–12 September 2017, (National Hurricane Center, Hurricane Irma Report, 2017).....	33
Figure 4.7. The central pressure observations for Hurricane Irma, (National Hurricane Center, Hurricane Irma Report, 2017).....	34
Figure 4.8. The surface wind speed observations for Hurricane Irma, (National Hurricane Center, Hurricane Irma Report, 2017).....	34
Figure 4.9. Damage caused by Hurricane Irma in the Caribbean Islands, (National Hurricane Center, Hurricane Irma Report, 2017).....	35
Figure 4.10. Bathymetries used for numerical modeling of Hurricane Irma a) coarse bathymetry b) nested bathymetry. The horizontal coordinates represent longitude in degree (East) and the vertical coordinates represent for latitude (North).....	37
Figure 4.11. a) The path of the hurricane Irma from NHC, Hurricane Irma Report,2017. b) The distribution of maximum water level between 02.09.2017 and 11.09.2017, due to atmospheric pressure and wind change during Hurricane Irma	

event and the path of the hurricane taken from NHC Hurricane Irma Report. For the simulation result, the horizontal coordinate represents longitude in degree (East) and the vertical coordinate represents for latitude (North) .....	38
Figure 4.12. The location of Antigua, Barbuda and Vieques Islands. The horizontal coordinate represents longitude in degree (East) and the vertical coordinate represents for latitude (North) .....	39
Figure 4.13. The numerical model results for a) Antigua, a) Barbuda and c) Vieques .....	41
Figure 4.14. The path of Hurricane Maria, 16–30 September 2017, National Hurricane Center, Hurricane Maria Report, 2017). .....	43
Figure 4.15. Pressure observations and central pressure curve for Hurricane Maria, 16–30 September 2017, National Hurricane Center, Hurricane Maria Report, 2017). .....	44
Figure 4.16. Wind speed observations and maximum sustained surface wind speed curve for Hurricane Maria, 16–30 September 2017, National Hurricane Center, Hurricane Maria Report, 2017). .....	44
Figure 4.17. Maria’s damage in Dominica, National Hurricane Center, Hurricane Maria Report, 2017). .....	45
Figure 4.18. Maria’s damage in Puerto Rico, National Hurricane Center, Hurricane Maria Report, 2017). .....	45
Figure 4.19. The path of Hurricane Maria, the data obtained from the NHC ( <a href="https://www.nhc.noaa.gov/">https://www.nhc.noaa.gov/</a> ) and tide gauge stations (triangles) used in Heidarzadeh et. al., 2018 are shown with name abbreviations: GDL1, Pointe à Pitre (Guadelou .	46
Figure 4.20. a) The path of the Hurricane Maria taken from NHC, Hurricane Maria Report, 2017. b) Distribution of maximum water level due to atmospheric pressure and wind during Maria and the path of the strom taken by NHC Hurricane Maria Report. The horizontal coordinate represents longitude in degree (East) and the vertical coordinate represents for latitude (North) .....	48

Figure 4.21. a) The original tide gauge records, b) The de-tided tide gauge waveforms, c) The one-hour averaged waveforms representing the storm surge amplitudes (Heidarzadeh et. al.,2018).....	49
Figure 4.22. The numerical model results for a) GDL1, Pointe à Pitre (Guadeloupe); b) GDL2, La Desirade Island (Guadeloupe); c) PTM, Portsmouth (Dominica); d) MRG, Marigot (Dominica); e) MTQ, Martinique (Fort de France) .....	52
Figure 4.23. The storm caused big waves in Bodrum, Mugla,Turkey (“Bodrum'da sađanak”, 2018) .....	53
Figure 4.24. The storm damage in Izmir, Turkey (“İzmir'deki fırtına”, 2018).....	54
Figure 4.25. The bathymetry used for numerical modeling of the storm. ....	55
Figure 4.26. The sea level elevation during storm in a) Izmir and b) Bodrum, Turkey .....	56
Figure 4.27. Sea Recedes at Akyaka, Turkey, (Ward, L., 2018).....	57
Figure 4.28. The bathymetry used for numerical modeling of the storm. ....	58
Figure 4.29. The numerical model results for a) Stazzo, Sicily; b) Nea Kios, Greece; c) Akyaka, Turkey .....	61

## **CHAPTER 1**

### **INTRODUCTION**

Long waves can be generated by several natural phenomena that occur from both above and under the ocean. Natural hazards like sub-marine landslides, earthquakes, and volcanic eruptions cause a disruption from under the ocean while change in atmospheric pressure cause a disruption from above the ocean.

2011 Earthquake and Tsunami occurred in Japan and other marine hazards (hurricane and storm events) occurred in the last decades raised the importance of unexpected disasters and draw the research directions of coastal and ocean engineers and professionals to focus also on the future projections on the occurrence and assessment of marine induced hazards. In addition, the potential climate change effects on the temporal and spatial distribution of marine hazards increases the importance of climatic effects on marine hazard and their impacts on coastal areas and coastal utilities.

Storms can be observed in many different types such as windstorm, cyclone, tornadoes, thunderstorm, snowstorm, rainstorm, ice storm, sandstorm, etc. Cyclone is simply a large wind system that rotates about a center of low atmospheric pressure. This large system of pressure and wind rotates in a counterclockwise direction on the northern hemisphere while It rotates in a clockwise direction on the southern hemisphere. Anti-cyclones have high pressure center, with the winds rotating clockwise on the northern part of the earth and counterclockwise on the southern part of the earth. During cyclone events and storms, an abnormal rise of water level can be observed. The change in air pressure during storm events can cause the displacement

of water body and increase or decrease in water level. This water level has a mechanism of long waves (similar with tsunamis) and is called as storm surge. During cyclone events, the flooding, storm surge and strong winds occurred and can cause loss of lives and properties on coastal areas. Mel (2013) states that for the coastal areas exposed to tropical cyclones, storm surge events are the major hazards. The high water levels associated with storm surge that occur over short periods (few minutes) are generally recognized and understood. However, the high water levels associated with storm surge that can last a couple of days are not (World Meteorological Organization, 2011).

Tropical cyclone is simply a low-pressure system with rotating surface wind circulation over tropical or subtropical waters. Tropical Cyclone has specific names for different part of the world, depending on where in the world they are born. They are named in the western Pacific, tropical Atlantic and northern Indian oceans as hurricanes, in the eastern Pacific Ocean as typhoons; and in the Indian oceans and the southern Pacific as cyclones. The distribution of tropical cyclones around the world is given in Figure 1.1. The data is taken from NOAA's Historical Hurricane Tracks data base includes all the hurricane events since 1850.



*Figure 1.1. Tropical cyclone events around the world, (NOAA, Historical Hurricane Tracks data base)*

Hurricanes observed in Mediterranean region, also named as Medicanes are physically very similar to other tropical cyclones observed around the world (Romero and Emanuel, 2013). The frequency for the occurrence of Medicanes is low ( $1.57 \pm 1.30$  events per season). The Medicane season starts from August and ends in July of the following year, (Cavicchia et. al, 2013).

In this thesis, particularly water level increases caused by storm surge events are investigated by using numerical model NAMI DANCE. The temporal and spatial distribution of the atmospheric pressure and wind taken from different data sources are used as the input to the NAMI DANCE numerical model which solves Nonlinear Shallow Water Equations (long wave equations) for tsunami simulations. The numerical model applied to selected cyclonic events, 30 August–12 September, 2017 Hurricane Irma and September 16-21, 2017 Hurricane Maria from Atlantic region; January 18, 2018 Aegean Storm and September 29-30 2018 Medicane from Mediterranean region. The simulation results were compared with the observed values.

In Chapter 2, different approaches related with storm surge modeling are covered by reviewing the literature. In Chapter 3, the information about the NAMI DANCE tsunami model is given and the storm surge modeling process with the modifications applied on NAMI DANCE numerical model are explained. In Chapter 4, verification and validation tests are conducted and the results of the calculations of the numerical model are shown. Finally, Chapter 5 provides general summary, discussions of conclusions and future recommendations.



## CHAPTER 2

### LITERATURE SURVEY

#### 2.1. Long Waves Generated by Atmospheric Pressure Forcing

The pressure forcing long waves have been observed all over the world. The effective factors in the generation mechanism of the phenomenon have been studied and analyzed in scientific literature all around the world. Some of the studies about atmospherically induced long waves given as follows: Rabinovich et. al., (1998) and Monserrat et. al. (1991), the Balearic and Kuril Islands; Šepić et. al. (2015), Mediterranean and Black Sea; Jansa et. al., 2007, Ciutadella.

Hibiya and Kajiura (1982) made investigation about the “Abiki” phenomenon. Abiki is the name of the large oscillations of water level that is observed in Japan. On March 31, 1979, the water level increased up to 2.78 m at the tide station in Nagasaki Bay, Japan. They stated that during the Abiki event in Nagasaki Bay, a distinct atmospheric pressure disturbance with 3 mb was recorded at some of the neighboring stations. They examined the effect of the atmospheric pressure disturbance on the observed large range of oscillations using numerical simulation and confirmed the relation between the large oscillations of water level in the bay and the moving pressure in the atmosphere. For numerical modeling, they used linearized, depth-integrated shallow water equations for an inviscid fluid. In the equations 2.1,2.2 and 2.3, they substitute  $\eta^* = -p/(\rho g)$  into the shallow water equations of motion and continuity where  $p$  represents the atmospheric pressure at the sea surface,  $g$  represents the acceleration due to gravity and  $\rho$  represents the density of sea water. In the given equations below,  $x$  and  $y$  coordinates represent the horizontal while  $z$  coordinate represents the vertical

coordinate,  $Q_x$  and  $Q_y$  represent the depth-integrated transport components,  $h$  represent the depth of the sea,  $\eta$  represents the relative water surface elevation.

$$\frac{\partial Q_x}{\partial t} = -gh \frac{\partial}{\partial x} (\eta - \eta^*) \quad (2.1)$$

$$\frac{\partial Q_y}{\partial t} = -gh \frac{\partial}{\partial y} (\eta - \eta^*) \quad (2.2)$$

$$\frac{\partial \eta}{\partial t} = - \left( \frac{\partial Q_x}{\partial x} + \frac{\partial Q_y}{\partial y} \right) \quad (2.3)$$

The grid intervals used for the model are 4 km and 2 km with 3 sec time interval ( $\Delta t$ ). The pressure wave at the sea surface linearly increased up to  $\Delta p = 3$  mb and with a constant speed of 31.33 m/sec. They confirmed that the results of the numerical model matched with the tide gauge values.

An et. al. (2012) made numerical experiments. They solve the linear shallow water equations to obtain the effect of physical parameters of storms to the generated edge waves. They used COMCOT numerical model (cornell multi-grid coupled Tsunami model) to examine the relationship between storm parameters (moving atmospheric pressure distribution) and generated waves. COMCOT model was originally developed to simulate long wave propagation caused by earthquake generated tsunamis was developed by by Xiaoming Wang, Y. S. Cho, S. B. Woo (Wang, 2009). The model uses the leap-frog finite-difference algorithm. However, COMCOT model has been expanded to simulate different wave generation mechanisms. The linear shallow water equations used in the generation of long waves are expressed in Equations 2.4, 2.5 and 2.6. In the Equations, P and Q represent the depth averaged

horizontal volume fluxes,  $h$  represents the water depth,  $\eta$  represents the free surface elevation,  $p_a$  represents the pressure distribution in the atmosphere and  $u$  and  $v$  represent horizontal velocity (the depth averaged).

$$\frac{\partial \eta}{\partial t} + \frac{\partial P}{\partial x} + \frac{\partial Q}{\partial y} = 0 \quad (2.4)$$

$$\frac{\partial P}{\partial t} + gh \frac{\partial \eta}{\partial x} = -\frac{h}{\rho} \frac{\partial p_a}{\partial x} \quad (2.5)$$

$$\frac{\partial Q}{\partial t} + gh \frac{\partial \eta}{\partial y} = -\frac{h}{\rho} \frac{\partial p_a}{\partial y} \quad (2.6)$$

They expressed the moving atmospheric pressure distribution along the shoreline in the Equation 2.7 and the phase speed of the generated edge when the wavelength of the generated edge wave is twice of the effective radius of the moving pressure distribution in the Equation 2.8. They also suggest a formula for the wavelength of the edge wave packet given in the Equation 2.9.

In the Equations 2.7, 2.8 and 2.9,  $p_0$  represents the atmospheric pressure and is taken as  $2 \times 10^3$  Pa,  $U$  represents the velocity of the pressure distribution in the alongshore direction,  $U_{cr}$  represents the phase speed of the generated edge wave,  $a$  is the effective radius of the moving atmospheric pressure distribution and  $t_0$  represents the prescribed time of the moving pressure.

The numerical model results states that if the speed of the design storm is greater than the critical speed that is given in the Equation 2.8., the wavelength of the generated

edge wave is independent of the storm size and can be determined by Eq. 2.9. The generated edge wave grows linearly in time and propagates to the coast from the behind of the center of the designed storm.

$$p_a = p_0 [1 - e^{-t/t_0}] \exp\left[-\frac{x^2 + (y - Ut)^2}{a^2}\right] \quad (2.7)$$

$$U_{cr} = \sqrt{\frac{ga\alpha}{\pi}} \quad (2.8)$$

$$\lambda = \frac{2\pi U^2}{g\alpha} \quad (2.9)$$

Kakinuma and Fukita (2012) made numerical simulation to analyze the causes of the large oscillations that reached up to 3 m on between February 24 and 26, 2009 in Urauchi Bay, Kyushu Island, Japan. To numerically simulate the waves, they applied the atmospheric pressure disturbance to the 2D nonlinear shallow water equations. The set of the equations are given in Equations 2.10, 2.11 and 2.12.

In the Equations 2.10, 2.11 and 2.12, U and V represent velocities in the x and y directions, P is atmospheric pressure on the surface of the water, f is the Coriolis coefficient which is taken as  $7.3 \times 10^{-5} \text{ s}^{-1}$  and K is the sea bed coefficient which is taken as  $2.6 \times 10^{-3}$ .

$$\frac{\partial \eta}{\partial t} + \frac{\partial}{\partial x} \{(\eta + h)U\} + \frac{\partial}{\partial y} \{(\eta + h)V\} = 0 \quad (2.10)$$

$$\begin{aligned} \frac{\partial U}{\partial t} + \frac{\partial U^2}{\partial x} + \frac{\partial(UV)}{\partial y} = fV - g \frac{\partial \eta}{\partial x} - \frac{1}{\rho} \frac{\partial P}{\partial x} + A_h \left( \frac{\partial^2 U}{\partial x^2} + \frac{\partial^2 U}{\partial y^2} \right) \\ - \frac{KU\sqrt{U^2 + V^2}}{\eta + h} \end{aligned} \quad (2.11)$$

$$\begin{aligned} \frac{\partial V}{\partial t} + \frac{\partial V^2}{\partial y} + \frac{\partial(UV)}{\partial x} = fU - g \frac{\partial \eta}{\partial y} - \frac{1}{\rho} \frac{\partial P}{\partial y} + A_h \left( \frac{\partial^2 V}{\partial x^2} + \frac{\partial^2 V}{\partial y^2} \right) \\ - \frac{KV\sqrt{U^2 + V^2}}{\eta + h} \end{aligned} \quad (2.12)$$

They also classified the atmospheric pressure into four patterns. For each pattern, evaluations are made and compared with the data taken from GPV. The pressure patterns are given in the Equations 2.13, 2.14, 2.15 and 2.16.

$$P(x, t_o) = \begin{cases} \frac{P \max}{2} \left\{ 1 + \cos \left[ \frac{2\pi}{L} (x - x_c) \right] \right\} & (|x - x_c| \leq L/2) \\ 0 & (|x - x_c| > L/2) \end{cases} \quad (2.13)$$

$$P(x, t_o) = P_0 \{1 - \sin[\pi(x - x_c)/L]\} / 2 \quad (2.14)$$

$$\begin{aligned} P(x, t_o) = P_0 \{1 + \cos[2\pi(x - x_c)/L]\} / 2 \\ + P_0 \{1 - \sin[\pi(x - x_c)/L]\} / 2 \end{aligned} \quad (2.15)$$

$$\begin{aligned} P(x, t_o) = 0.005e^K P_0 \{1 + \cos[6\pi(x - x_c)/L]\} / 4 \\ + P_0 \{1 - \sin[3\pi(x - x_c - x_d)/L]\} / 2 \end{aligned} \quad (2.16)$$

The numerical model results show that the harbor oscillation occurred on February 24 and 26, 2009 in Urauchi Bay should be generated by atmospheric pressure disturbance.

Monserrat et. al. (2006) showed the similarities between seismic and meteorological tsunamis by comparing the tsunami and meteotsunami events in the world. They analyze meteotsunami events in Nagasaki Bay, the Balearic Islands, Longkou Harbour and Adriatic Sea. They concluded that the waves generated by both tsunami and meteotsunami have similar physical properties, same periods and same spatial scales.

## 2.2. The Surface Wind Drag Coefficient

It is important to state that, in storm surge modeling, besides pressure parameter, the wind speed, direction and surface wind friction should also be included. In this section, the some of the studies about the surface drag coefficient values during storm are explained.

Taylor (1916) stated that local surface stress can be related to the surface wind speed, height and drag coefficient. In the equation,  $C_D$  is drag coefficient and it is related to aerodynamic roughness and stability parameter,  $V$  represents the wind speed on the surface at a height of  $z$  and  $\rho_{air}$  is air density.

$$\tau_0 = \rho_{air} C_D V z^2 \quad (2.17)$$

Garratt (1977) made observations of wind stress and profile. He used the Charnock's (1955) relation and express the neutral drag coefficient ( $C_{DN}$ ) in terms of wind speed at 10 m high from water level.

$$C_{DN}(10)x10^3 = 0.5W^{0.46} \quad (2.18)$$

$$C_{DN}(10)x10^3 = 0.75 + 0.067W \quad (2.19)$$

Zhang and Li (1996) used 2D model for storm surge calculations with third-generation wave model and compared the results with real cases occurred in South China Sea.

$$\tau = \rho C_D |U_{10}| U_{10} \quad (2.20)$$

$$C_D = (0.066|U_{10}| + 0.63)x10^{-3} \quad (2.21)$$

Powell et. al. (2003) made analysis about tropical cyclones wind profile data, and observed the change of wave-depended drag coefficient ( $C_D$ ) in tropical cyclones. They found that surface momentum flux decreases for the winds with the speed more than 25 m/s as the wind speeds increase above hurricane force.

Wrobel-Niedzwiecka et. al. (2019) compare the average flux values in the European Arctic and North Atlantic using seven different drag coefficient parameterization. They concluded that the differences between the drag coefficient parameterizations for the wind speed lower than 10 m/s are greater than for the wind speed higher than 10 m/s.

### **2.3. Storm Surge Modeling**

It is important to state that the studies on the forecasting of storm surge started in 1950s. At the present, there are different storm surge models that based on different approaches. However, approximately 75 percent of the reported operational or pre-operational applications are two-dimensional models (World Meteorological Organization, 2011).

SLOSH (Sea Lake Overland Surges from Hurricanes) is a two-dimensional numerical model. It is developed by FEMA (Federal Emergency Management Agency), the National Weather Service and United States Army Corps of Engineers based on the studies of Chester Jelesnianski on numerical modeling of storm surge (Jelesnianski et al., 1992). It is run by NOAA/NWS Meteorological Development Laboratory to estimate storm surge heights from predicted or historical storms. The model solves the depth-integrated shallow water equations by using storm parameters such atmospheric pressure level, speed, direction and size and wind speed and direction. Moreover, the astronomical tides can be included in the model by giving an initial tide level as an input. However, precipitation, river flow, or wind-driven waves are not included in the SLOSH model. The covered areas of the model are updated every year.

ADvanced CIRCulation (ADCIRC) model is a computer code that solves depth-integrated continuity equation using a finite-element solution in two and three dimensions. It can be run using cartesian and spherical coordinate system. Even though, there are other groups that involved in the development process, the initial developers of the code were Rick Luetlich from University of North Carolina and Joannes Westerink from University of Notre Dame. Other principal developers include Randall Kolar (University of Oklahoma at Norman) and Clint Dawson

(University of Texas at Austin). Various other groups are involved in development and support. ADCIRC can be used to predict flooding and storm surge, to model tides and wind forcing circulation for near shore marine operations (Luettich et al., 1992).

JMA model is a model used for storm surge calculations that solves the 2D shallow water equations using a finite difference method. It is run by the Japan Meteorological Agency (JMA) for storm surge warnings using the data taken from 290 points along the Japanese coastline. The astronomical tide for each station is added to the predicted storm surge (Higaki et. al., 2009).

HYPSE is one-layer nonlinear shallow water model that is developed using the depth average of the momentum equation with constant velocity profile. The basin of the model covers only Adriatic Sea (Lionello et al. 2005 and 2006).

SURGE is three dimensional hydrodynamic numerical model of ocean circulation developed by Blumberg and Mellor (1987). It is improved based on POM (Princeton Ocean Model). The numerical model can predict and simulate storm surge, flooding, water recession, over wash and associated horizontal currents. The wave effects, e.g., wave-enhanced surface stress, bottom friction and radiation stress are not included in the model.



## CHAPTER 3

### STORM SURGE MODELING

#### 3.1. NAMI DANCE Tsunami Model

NAMI DANCE is a tsunami numerical model that analyzes tsunami events and simulate tsunami propagation, evolution and inundation. The model has been developed by scientist Andrey Zaytsev, Ahmet. Cevdet Yalciner, Anton Chernov, Efim Pelinovsky and Andrey Kurkin as a collaboration of Ocean Engineering Research Center, Middle East Technical University, Turkey, and Special Research Bureau for Automation of Marine. Researches, Russia. NAMI DANCE is developed based on TUNAMI-N2.

The model solves the nonlinear shallow water equations by employing the explicit leapfrog finite difference. The nonlinear long wave equations are solved depending on the rectangular grids by considering related boundary conditions. The numerical model can form tsunami source by rupture characteristics given as an input or by pre-determined wave form. NAMI DANCE can compute wave propagation, arrival time, coastal amplification, inundation, distribution of water surface elevations at sea state, discharge fluxes, current velocities and their directions at selected time intervals, drag force and impact force and relative damage levels, time histories of eta at selected gauge locations. In addition to that, the model can plot sea state at selected time intervals in 3D from different camera and light positions and make animation of tsunami propagation between source and target regions (Yalciner et. al., 2006b, 2007b). NAMI DANCE also used with nested grid domains, which the grid size ratio from parent to child domain is suggested to be less than 10. Several tsunami events

have been modeled by applying NAMI DANCE in more than 10 institutes worldwide (Zaitsev et al., 2008; Yalciner et al., 2010, 2012).

Moreover, NAMI DANCE were tested for surge and coastal inundation at the Black Sea coast of Turkey by Aydın (2016). The NAMI DANCE numerical model is coupled with ADCIRC and SWAN numerical models. The wave parameters obtained from ADCIRC and SWAN used in NAMI DANCE to investigate coastal flooding caused by the storm event occurred between 23-26 September 2014 in Giresun, Turkey.

NAMI DANCE were also tested by Metin (2016) to investigate the effects of the movement of an atmospheric pressure on the large wave oscillations in a region with no storm or seismic activity.

The phases of implementation for NAMI DANCE numerical model are given in Figure 3.1.

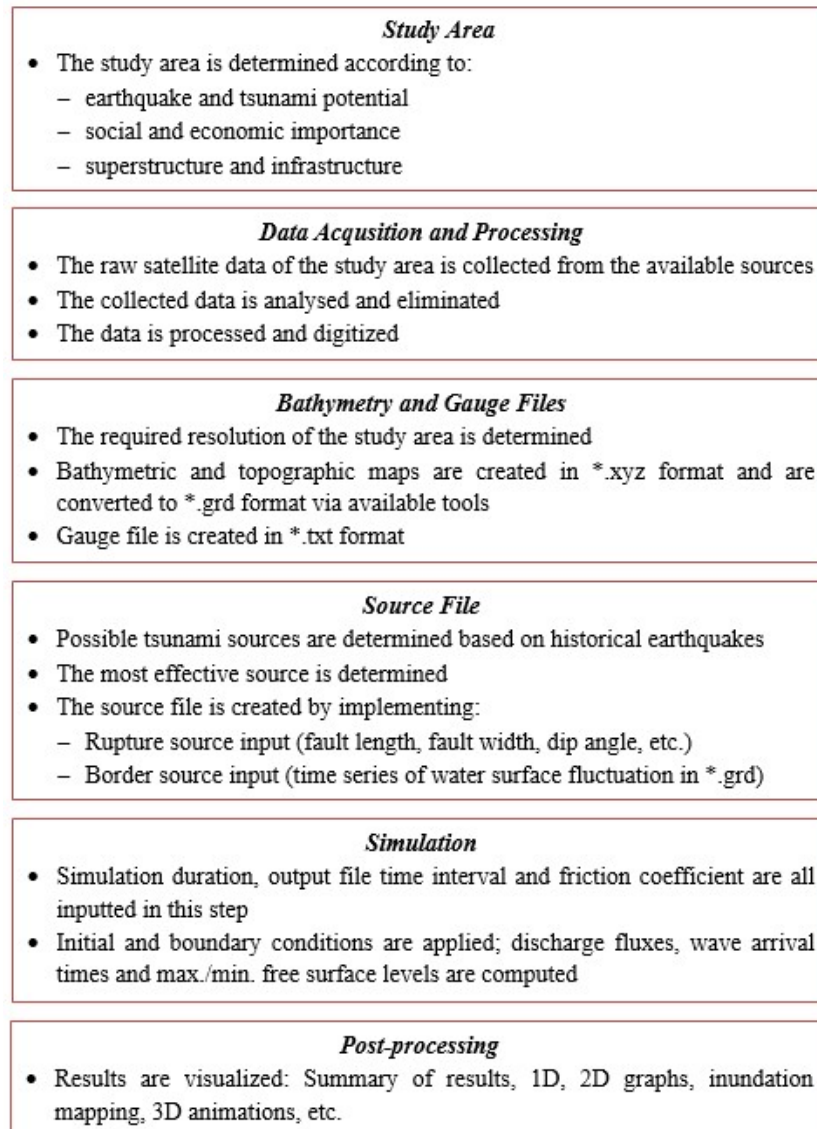


Figure 3.1. Modeling process of NAMI DANCE (Velioglu, 2017)

The validation and verification of storm surge modeling process are carried out using NAMI DANCE numerical model. For storm surge modeling applications, pressure and wind parameters are added to the long wave equations as it is given in Chapter 4.

### **3.2. Storm Surge Modeling with NAMI DANCE**

Zone of low pressure in atmosphere can cause large scale of air mass to rotate around its center and create zone of low pressures with inward spiral anticlockwise (northern hemisphere) or clockwise (southern hemisphere) winds circulation. The water level increases at the low pressure regions, in contrary it decreases at high pressure regions. This phenomenon causes unbalanced water level in ocean area which generates long wave. Other phenomena causing long wave generation is to transfer the energy gained by some outer forcing by wind, tide and tsunami, spatial and temporal large scale atmospheric pressure disturbances. The generated long wave propagates in all direction. When storm is large enough, water body formed by pressure drop or rise in the atmosphere, propagates towards shallow areas and can generate large water level fluctuations and cause damage the coastal areas. This phenomenon is named as storm surge. In other words, storm surge is the increase or decrease in water level generated by the atmospheric forcing (World Meteorological Organization, 2011).

It should be noted that atmospheric pressure disturbances are highly related with temperature, altitude and air density. Due to the fact that, the density of the cold air is greater, and decrease in temperature causes the air in the atmosphere drop, as a result, low temperatures generates high air pressures while high temperatures generates low air pressures. Over the ocean, low pressure in the atmosphere leads to a static water level rise while high pressure in the atmosphere leads to a static water level drop. Pugh, 2004 indicates that in general, 1 mbar pressure difference in the atmospheric pressure cause nearly 1 cm water level rise in the mean sea elevation.

The waves generated by these kinds of atmospheric effects (storm surge) are called long waves which have a period of several hours to one day depend on bathymetric conditions and the energy gained by pressure. The length of the generated wave equals

to the width of the pressure center of the storm. As a result, these type of waves are calculated using the shallow water equations.

In storm surge analysis, there are two major components atmospheric pressure distribution and wind direction and speed. As a result, in the storm surge calculations, the temporal and spatial distribution of air pressure, wind speed and direction on the water surface, and wind friction (between air and water) with the path the storm should be known. In addition to these components, it should be noted that the change of wave characteristics during propagation towards coast due to bathymetric and morphological conditions have important roles on the nearshore characteristics of storm surge. These factors with other important components are provide with short descriptions in the Table 3.1. Also, a diagram of various physical processes that can be effective during storm surge is shown in Figure 3.2 (Alymov, 2005).

*Table 3.1. Wave Components effective in storm surge (Ergin,2010)*

<b>Wave Shoaling</b>	Waves start feeling the sea bed at intermediate depth where $d/L_0 \leq 0.5$ , when they are propagating towards shallow areas with their crest lines parallel to bottom contours.
<b>Wave Refraction</b>	When waves enter into transitional depth with crest lines not parallel to bottom contours, their propagation directions change depending on the bottom topography (i.e. the variations of sea depth).
<b>Wave Breaking</b>	Wave heights change as the waves propagates towards the shore by the combined effects of refraction and shoaling. Continuous increase in wave height observed lead to speed of the water particles at

	the wave crest become greater than the average celerity of the wave profile. As a result, when the wave propagates towards the shore, it starts to break.
<b>Wave Setup</b>	The increase in the mean water level caused by the continuous wave breaking action is called the wave set-up.
<b>Currents</b>	The directed movement of water that flows in one of the Earth's oceans. The currents can be permanent or continuous and they are generated due to the earth's rotation, the gravitation of the moon, the wind, the temperature and salinity differences.
<b>Tides</b>	The sea surface rises and falls regularly ones or twice a day. This periodic motion is called tidal motion. It is sometimes called the astronomical tide

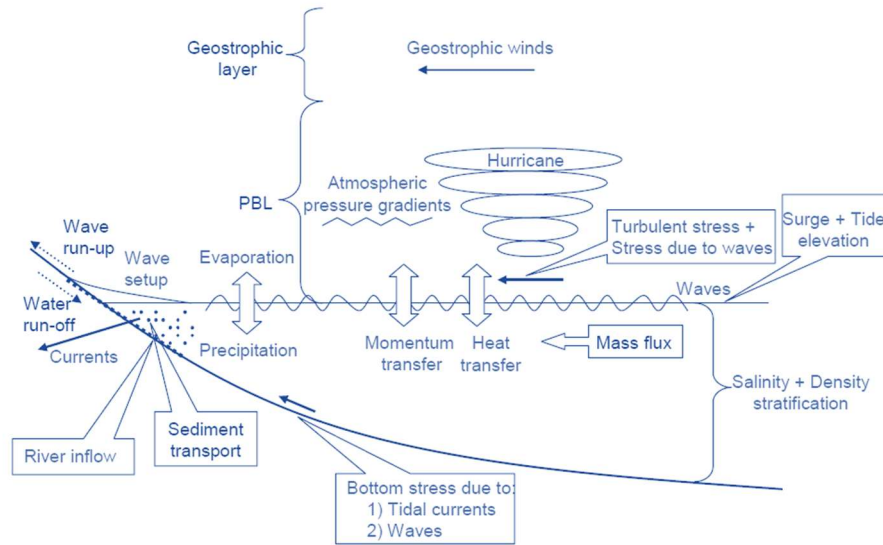


Figure 3.2. A diagram of various physical processes (Alymov,2005).

Since, the waves generated by storm surge are long waves, it can be expressed with 2D depth averaged shallow water equations. The governing equations of 2D nonlinear depth averaged shallow water equations are given in Equations 3.1-3.7 (Probst and Franchello, 2012).

In the Equation 3.1,3.2,3.3 and 3.4,  $U$ ,  $F$  and  $C$  are respectively the source, flux and conservative vectors,  $v_x$  and  $v_y$  are the velocity of the fluid for  $x$  and  $y$  directions respectively,  $h$  signifies the depth of the water,  $z$  represents the vertical coordinate of the bottom,  $g$  the gravitational acceleration (opposite to the  $z$  direction) and  $S_f$  represents the bottom friction that is calculated using the Manning formula,  $q$  is precipitation,  $f$  is the coriolis force that is taken as  $f = \omega \sin \theta$ ,  $S_p$  and  $S_u$  signifies for the pressure and wind source for  $x$  and  $y$  directions.

$$\frac{\partial U}{\partial t} + \Delta F = C \quad (3.1)$$

$$U = \begin{Bmatrix} h \\ h v_x \\ h v_y \end{Bmatrix} \quad (3.2)$$

$$F = F_x + F_y \quad \text{where } F_x = \begin{Bmatrix} h v_x \\ h v_x^2 + gh^2 / 2 \\ h v_x v_y \end{Bmatrix} \quad F_y = \begin{Bmatrix} h v_y \\ h v_y^2 + gh^2 / 2 \\ h v_y v_x \end{Bmatrix} \quad (3.3)$$

$$C = \begin{Bmatrix} q \\ hf v_y - gh (\partial z / \partial x + S_{fx} + S_{px} + S_{ux}) \\ -hf v_x - gh (\partial z / \partial x + S_{fy} + S_{py} + S_{wy}) \end{Bmatrix} \quad (3.4)$$

The bottom friction source parameter can be expressed by the Manning formula which Manning's coefficient is represented by n and it can be calculated by using the Equation 3.6. In the Manning formula D represents for the water depth.

$$S_f = \{S_{fx}, S_{fy}\} = \frac{n^2 \sqrt{v_x^2 + v_y^2}}{h^{4/3}} \{v_x, v_y\} \quad (3.5)$$

$$n = \frac{\sqrt{f(\eta + D)^{1/3}}}{2g} \quad (3.6)$$

The pressure and source parameters added to include the atmospheric forcing in the long wave equation. In the Equations 3.7 and 3.8,  $\rho_w$  represents the density of water,  $\rho_{air}$  is the density of air,  $U_{10}$  is the wind velocity for x and y direction which is

measured from 10 m above of the sea surface,  $C_D$  represents the drag coefficient and  $P$  represents the atmospheric pressure.

$$S_p = \{S_{px}, S_{py}\} = \frac{1}{\rho_w g} \left\{ \frac{\partial P}{\partial x}, \frac{\partial P}{\partial y} \right\} \quad (3.7)$$

$$S_u = \{S_{ux}, S_{uy}\} = \frac{\rho_{air} C_D}{\rho_w} \frac{\sqrt{U_{10x}^2 + U_{10y}^2}}{h} \{U_{10x}, U_{10y}\} \quad (3.8)$$

In the Figure 3.3, the coordinate and variables of the shallow water model are given schematically where  $h$  represents for the depth of water,  $z$  is the coordinate for vertical axes and  $\eta$  signifies for the free surface elevation.

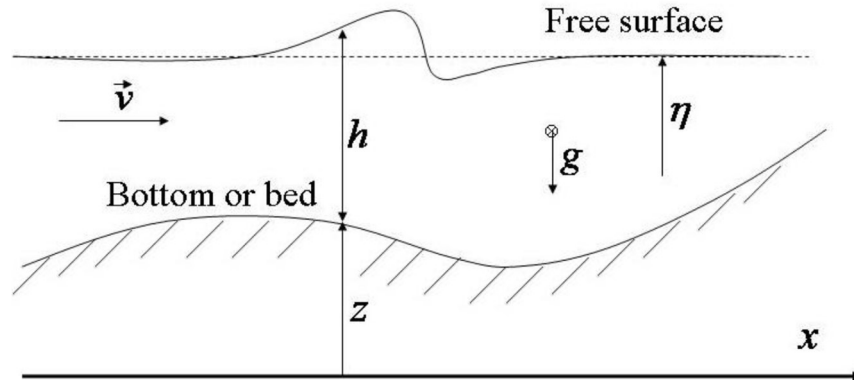


Figure 3.3. The variables of the shallow water model and their coordinates (Probst and Franchello, 2012).

Sorensen (2006) states that in numerical modeling, the selected area should be divided into square or rectangular segments. The long wave equations or shallow water equations should be written in finite difference form to apply to each square or rectangular grid in the selected area. For each segment, the appropriate boundary conditions must be applied. In general, there can be several boundary conditions to

allow correct computation of flow of water. These boundary conditions are water–land boundaries, low-lying areas which can cause flooding, barriers like islands and dikes which can be overtopped, inflow coming from outlet of rivers and surface runoff and offshore boundaries.

Monserrat et al., (2006) states that if the forcing comes from atmospheric pressure is known, the numerical modeling of long waves caused by pressure forcing is straightforward. Since, the ocean wave generated by pressure disturbance is first order, the 2D shallow water equations can be applied as in tsunami numerical modeling.

The storm surge phenomena implemented in the tsunami numerical model NAMI DANCE by Bora Yalciner (Yalciner et al., 2019), which have already solved the nonlinear form of vertically averaged shallow water equations. The model code includes tidal motion, coriolis force and bottom friction, however, it excludes radiation stresses.

The final form of the governing equations used in the new version of NAMI DANCE numerical modeling using mass and momentum conservation equations are given in the equations below.

$$\frac{\partial \eta}{\partial t} + \frac{\partial M}{\partial x} + \frac{\partial N}{\partial y} = 0 \quad (3.9)$$

$$\begin{aligned} & \frac{\partial M}{\partial t} + \frac{\partial}{\partial x} \left( \frac{M^2}{D} \right) + \frac{\partial}{\partial y} \left( \frac{MN}{D} \right) + gD \frac{\partial \eta}{\partial x} + \frac{\tau_x}{\rho_w} + \frac{D}{\rho_w} \frac{\partial P_{atm}}{\partial x} \\ & - \frac{\rho_{air} C_D}{\rho_w} U_{w10} \sqrt{U_{w10}^2 + V_{w10}^2} = 0 \end{aligned} \quad (3.10)$$

$$\begin{aligned} & \frac{\partial N}{\partial t} + \frac{\partial}{\partial x} \left( \frac{MN}{D} \right) + \frac{\partial}{\partial y} \left( \frac{N^2}{D} \right) + gD \frac{\partial \eta}{\partial y} + \frac{\tau_y}{\rho_w} + \frac{D}{\rho_w} \frac{\partial P_{atm}}{\partial y} \\ & - \frac{\rho_{air} C_D}{\rho_w} V_{w10} \sqrt{U_{w10}^2 + V_{w10}^2} = 0 \end{aligned} \quad (3.11)$$

In the Equations 3.9-3.10, M and N represent the discharge flux in the x and y directions respectively, t represents time,  $\eta$  represents water surface elevation, D represents the water depth,  $\rho_w$  represents the density of water,  $\rho_{air}$  represents the density of air,  $P_{atm}$  represents the atmospheric pressure in Pascal,  $C_D$  represents the drag coefficient and U and V represent the wind velocities measured 10 m above from the water surface in x and y directions, respectively. It should be noted that, the standard atmospheric pressure is taken as 1013 mbar in the computation.

The discharge fluxes are given in the Equations 3.12 and 3.13. In the equations, u and v represent the current velocities in x and y directions. For the horizontal wind velocity smaller or equal than 26 m/s, the drag coefficient is taken as it is indicated in Garrat (1977). For the horizontal wind velocity higher than 26 m/s, the drag coefficient is taken as constant (Powell et. al., 2003).

$$M = \int_{-h}^{\eta} u dz = u(D + \eta) = uD \quad (3.12)$$

$$N = \int_{-h}^{\eta} v dz = v(D + \eta) = vD \quad (3.13)$$

$$C_D = \left\{ \begin{array}{l} (0.75 + 0.067U_{w10}) * 10^{-3}, \text{ for } U_{w10} \leq 26m / \text{sec} \\ 2.18 * 10^{-3}, \text{ for } U_{w10} > 26m / \text{sec} \end{array} \right\} \quad (3.14)$$

$\tau_x$  and  $\tau_y$  represent the bottom shear stresses in the x and y directions respectively. They are given in the following equations.

$$\frac{\tau_x}{\rho} = \frac{fn^2}{(\eta + D)^{7/3}} M \sqrt{M^2 + N^2} \quad (3.15)$$

$$\frac{\tau_y}{\rho} = \frac{fn^2}{(\eta + D)^{7/3}} N \sqrt{M^2 + N^2} \quad (3.16)$$

As an Input, the specified bathymetry for the study domain with sufficient grid size, the atmospheric pressure field at sea level, the wind velocity for 10 m above from sea surface in x and y direction and tide level (optional) should be given. As an output, NAMI DANCE storm surge model computes distribution of water elevations at the surface (sea state), inundation, distribution of current velocities and their directions and discharge fluxes at selected time intervals.

## CHAPTER 4

### VALIDATION AND VERIFICATION OF NUMERICAL MODEL

#### 4.1. Verification and Validation Procedures in Modeling

Verification and validation procedures (the V&V process) are essentially required to assess accuracy and credibility of a numerical model.

During the development stage of a numerical model, verification tests ensure that the numerical model meet with the specified requirements or represents the conceptual description of the model. On the other hand, validation tests ensure that the end result meet with the expectations or in this study, the model provide representation of the real world. In the Figure 4.1, the model verification and validation processes are shown.

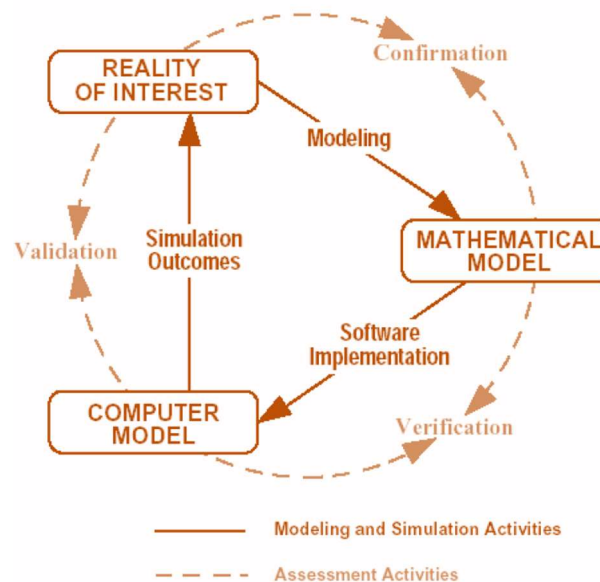


Figure 4.1. The model verification and validation process (Schlesinger, 1979).

## 4.2. Verification by Static Pressure Conditions in Regular Shaped Basin

Verification calculations for the numerical model are done to ensure that the numerical model can calculate the water elevations at the surface due to the effect of pressure disturbances in the atmosphere. The model is verified by applying static atmospheric pressure disturbances for regular shaped flat bathymetry.

### 4.2.1. Verification by Static Circular Low Pressure Condition (Cyclone Condition)

To observe the water level change due to low pressure forcing, regular shaped rectangular 128x128 flat bathymetry with 788 m grid size is selected (Figure 4.2). For the pressure difference, circular static pressure with 973 mbar at the center is applied on the 1013 mbar standard pressure condition after 4th hour. The change of water elevation at the center is given in the Figure 4.3.

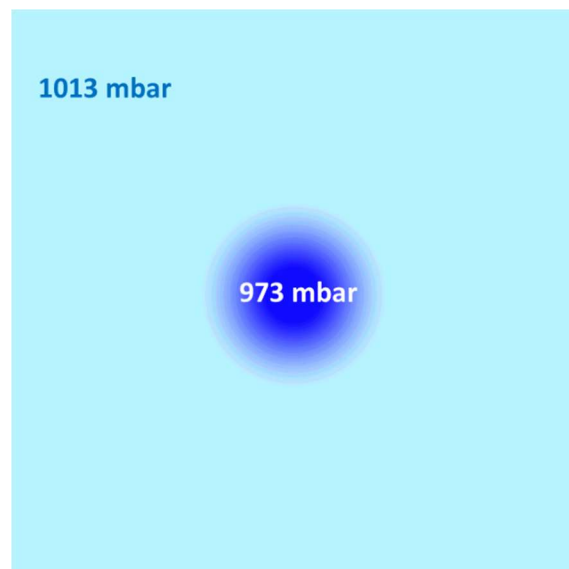


*Figure 4.2. Bathymetry with low pressure at the center*

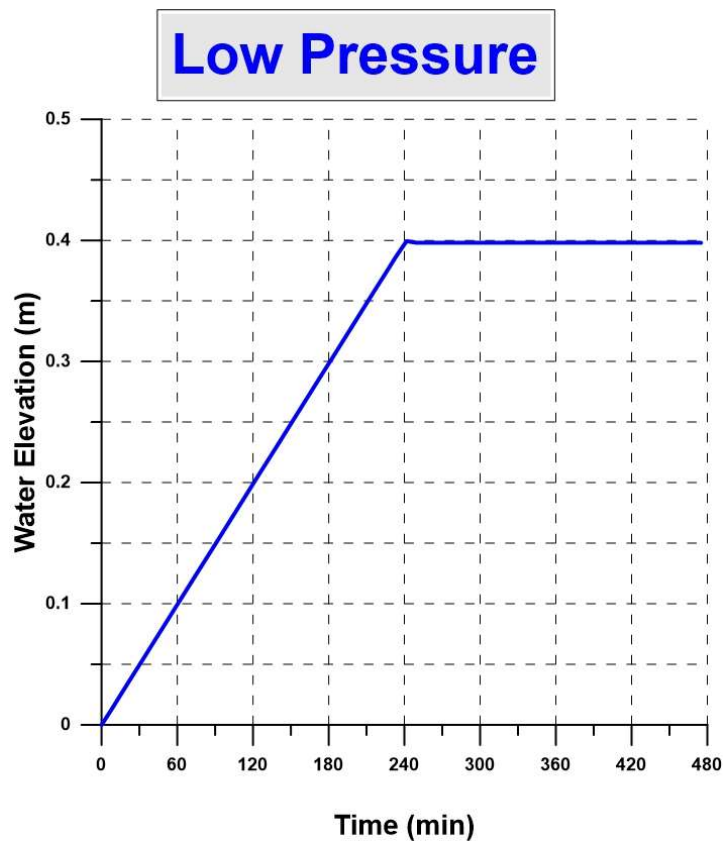


Figure 4.3. Water elevation change at the center due to low pressure

The water level rise is expected as 40 cm at the central point. As it can be seen from the Figure 4.3, during simulation, at first, the water level was stable, however, after pressure change from 1013 mb to 973 mb in the center of the domain. The water level increases to 40 cm. As it is indicated in Pugh's study (2004) that 1 mb pressure difference cause 1 cm water level rise, in the simulation, 40 mb pressure difference result in 40 cm sea level rise. Thus, the results fits well with the expectations.

#### **4.2.2. Verification by Static Circular High Pressure Condition (Anticyclone Condition)**

To observe the water level change due to high pressure forcing, same bathymetry is used in the test. For the pressure difference, circular static pressure with 1053 mbar at the center is applied on the 1013 mbar standard pressure condition after 4th hour. The change of water elevation at the center is given in the Figure 4.5.



*Figure 4.4. Bathymetry with high pressure at the center*

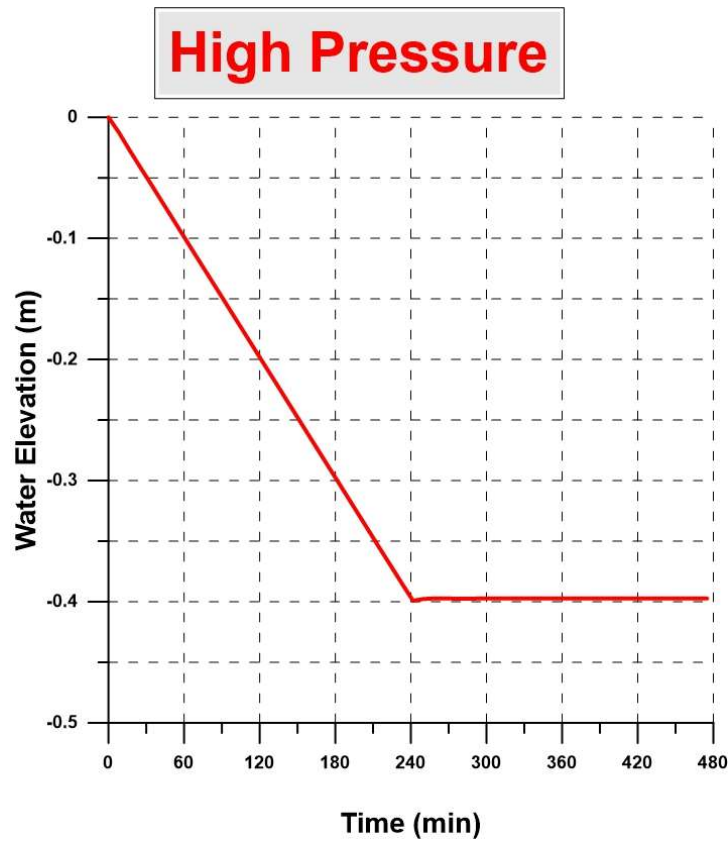


Figure 4.5. Water elevation change at the center due to high pressure

The water level drop is expected as 40 cm at the central point. As it can be seen from the Figure 4.5, during simulation, at first, the water level was stable, however, after pressure change from 1013 mb to 1053 mb in the center of the domain. The water level decreases to -40 cm. As it is indicated in Pugh's study (2004) that 1 mb pressure difference cause 1 cm water level rise, in the simulation, 40 mb pressure difference result in 40 cm sea level drop. Thus, the results fits well with the expectations.

### **4.3. Application to Case Studies**

Different validation tests of NAMI DANCE are performed by applications to numerous case studies. The results of numerical model simulation are compared with the measurements and observations from the recent real cases from Caribbean and Mediterranean regions.

In September 2017, two strong hurricanes (Irma and Maria) occurred in Caribbean region. On January 18, 2018 and September 30, 2018 are the other cyclone like storm events occurred in Mediterranean region. In the following, these events are described and the validations of numerical model NAMI DANCE by applications to these events are given with comparisons.

#### **4.3.1. Application to 30 August–12 September, 2017 Cyclone Irma event**

Irma originated from the west coast of Africa. Along its path, the Hurricane Irma caused serious damage. In the Figure 4.6 the path of the hurricane is provided.

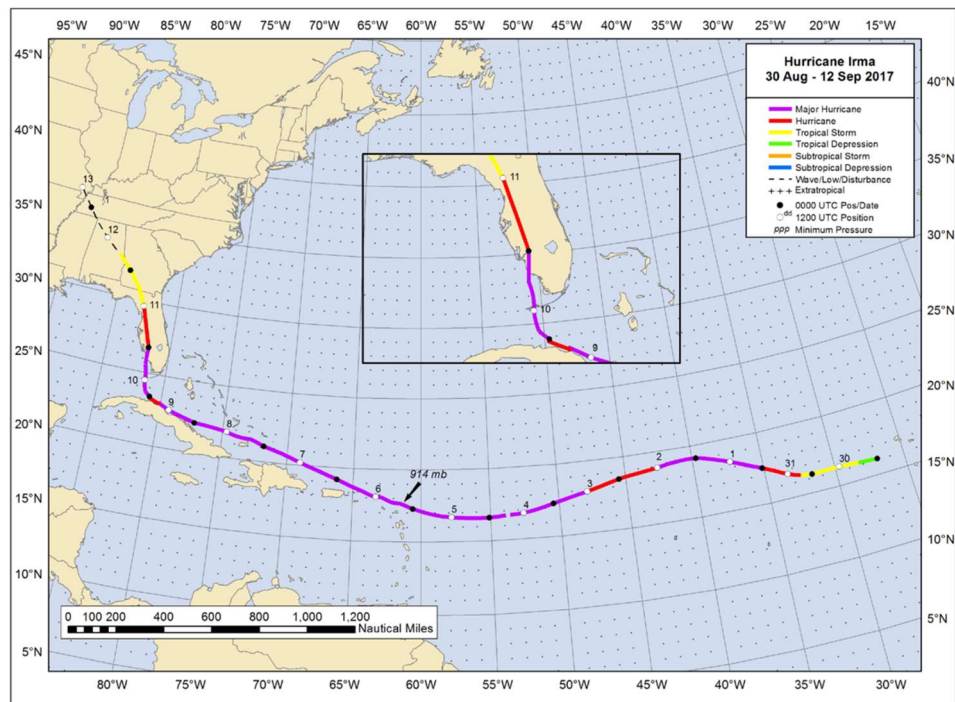


Figure 4.6. The path of the Hurricane Irma, 30 August–12 September 2017, (National Hurricane Center, Hurricane Irma Report, 2017).

The circulation system made seven landfalls with four of which occurred across the northern Caribbean Islands as a category 5 hurricane according to the Saffir-Simpson Hurricane Wind Scale (SFMR).

Based on surface wind estimates done by SFMR and flight-level winds observed by the Air Force Reserve and NOAA, Hurricane Irma had reached its peak intensity between 5 September to 6 September. On 6 September, the observed minimum central pressure was 914 mb at 06:00 UTC (Figure 4.7). In the Figure 4.8, Irma’s estimated peak intensity was around 155 kt (80 m/s) between 5 September and 6 September, 2017 (National Hurricane Center, Hurricane Irma Report, 2017).

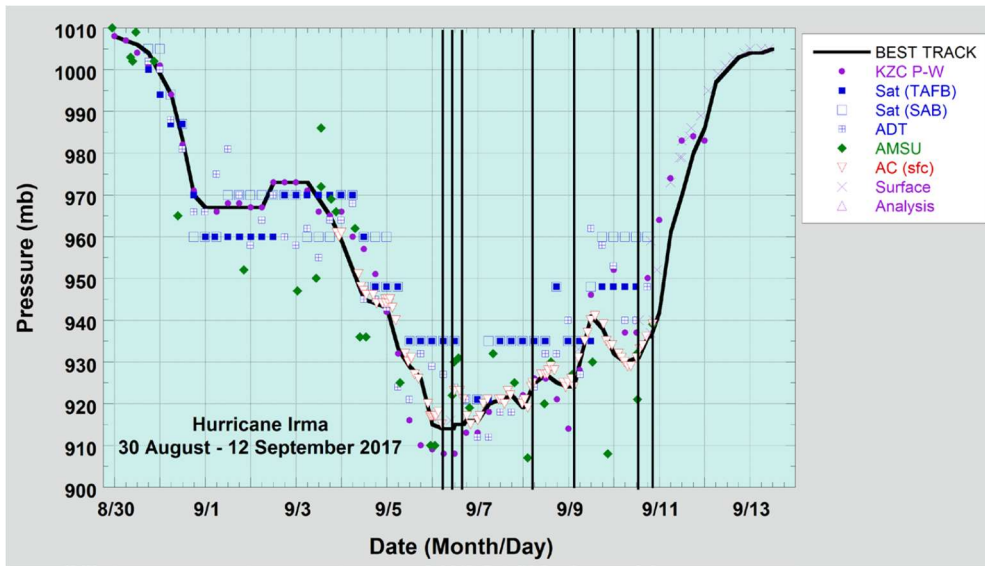


Figure 4.7. The central pressure observations for Hurricane Irma, (National Hurricane Center, Hurricane Irma Report, 2017).

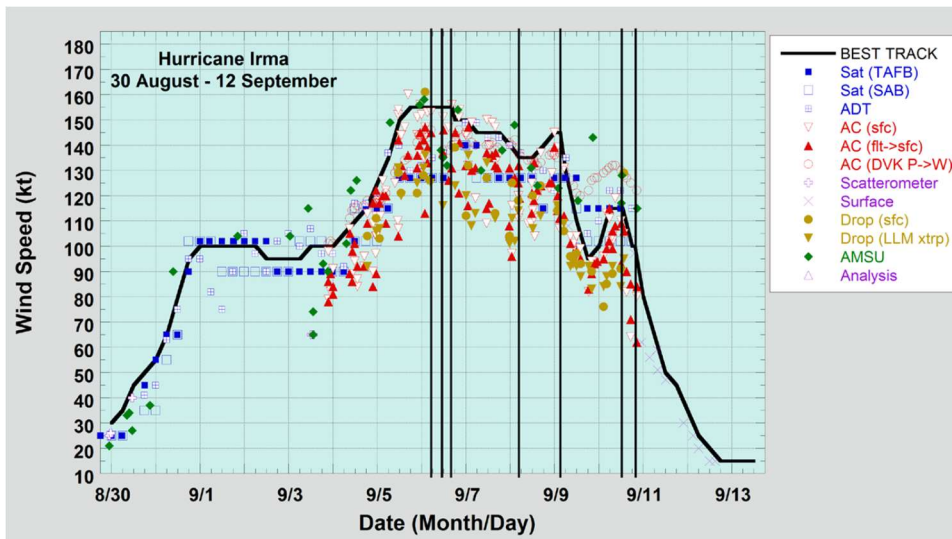


Figure 4.8. The surface wind speed observations for Hurricane Irma, (National Hurricane Center, Hurricane Irma Report, 2017).

Irma's strong winds, heavy rains, and storm surge caused 47 direct deaths. The most of the damage occurred in the Caribbean Islands (Figure 4.9).



Figure 4.9. Damage caused by Hurricane Irma in the Caribbean Islands, (National Hurricane Center, Hurricane Irma Report, 2017).

The storm surge generated by Hurricane Irma affected Caribbean Islands, Puerto Rico, Florida, Georgia and South Carolina and caused inundation and damages along the coast. On 6 September, Irma made landfall on Barbuda Island and Antigua Island as a category 5 hurricane that caused significant storm surge with maximum water level of 2.4 m Mean Higher High Water (MHHW). Along the coast of Vieques, Puerto Rico, Hurricane caused storm surge with around 0.4 m. Maximum inundation levels above the ground level recorded as 0.3 to 0.6 m.

In Table 4.1, the observed extremes of pressure, wind and storm surge level with the occurrence time for the selected NOAA stations are presented. As seen from Table 4.2, the minimum pressure reached 916.1 mb on September 06 at 05:36 (UTC). The maximum wind speed as gust, reached 71.5 m/s on September 06 at 04:54 (UTC). The maximum water level of increase was observed as 2.4 m in Antigua and Barbuda. In Vieques Island, Puerto Rico, the minimum pressure reached 991.9 mb on September 06 at 20:06 (UTC). The maximum wind speed as gust, reached 28.8 m/s on September 06 at 04:54 (UTC). The maximum water level was observed as 0.4 m. It should be

noted that, the observed water level values from NOAA’s stations include storm surge level due to pressure and wind as well as other phonemes such as wave set up, wave run up and tide.

*Table 4.1. The surface observations from selected land stations, National Hurricane Center, Hurricane Irma Report, 2017*

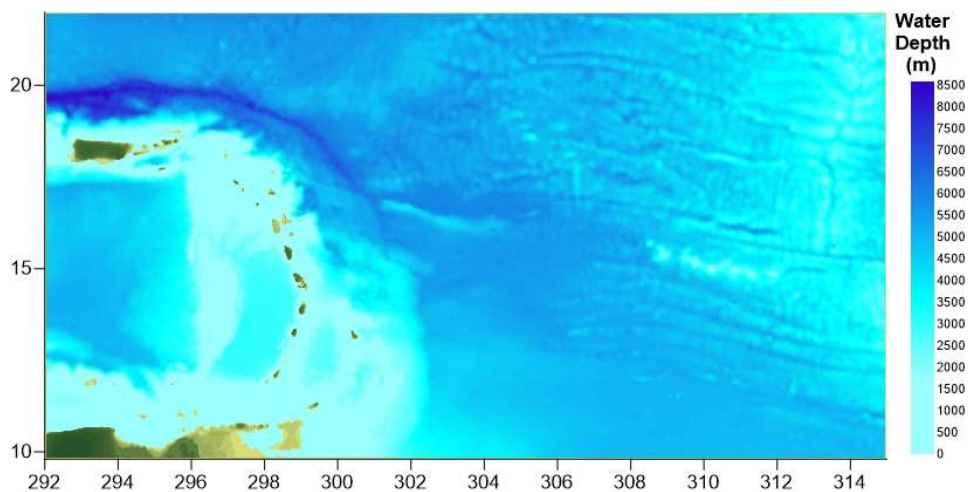
Location	Minimum Sea Level Pressure		Maximum Surface Wind Speed		Storm surge (m)
	Date/ time (UTC)	Press. (mb)	Date/ time (UTC)	Gust (m/s)	
Antigua and Barbuda	06/ 05:36	916.1	06/ 04:54	71.5	2.4
Vieques Island, Puerto Rico	06/ 20:06	991.9	06/ 21:30	28.8	0.4

Mean sea level pressure data and wind data with 10 m high above the sea level are taken from CFSR (Climate Forecast System Reanalysis), with 0.50°x0.50° (degree) grid size and 1 hr time period. The pressure and wind distributions on September 06, 2017 at 05:00 UTC taken from CFSR are given in the Appendix Figure A1 as an example.

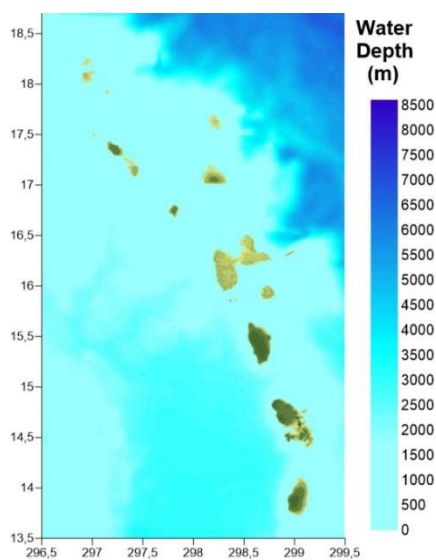
For Hurricane Irma, coarse bathymetry with 900 m grid size and nested bathymetry with 200 m grid size are selected. The bathymetry data is provided by GEBCO. The pressure and wind fields are inputted with 1hr intervals in the duration between 02.09.2017-11.09.2017 (9 days). The grid size and corner coordinates of the coarse and nested domains are given in the Table 4.2 and the bathymetries are shown in Figure 4.10.

Table 4.2. Detailed information about selected domains

Bathymetry	Grid Size (m)	Corner Coordinates			
Coarse Bathymetry	900	292E	315E	9.8N	22N
Nested Bathymetry	200	296.5 E	299.5E	13.5N	18.7N



(a)



(b)

Figure 4.10. Bathymetries used for numerical modeling of Hurricane Irma a) coarse bathymetry b) nested bathymetry. The horizontal coordinates represent longitude in degree (East) and the vertical coordinates represent for latitude (North).



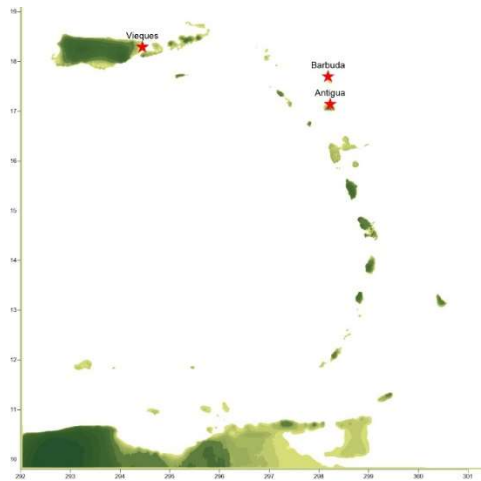
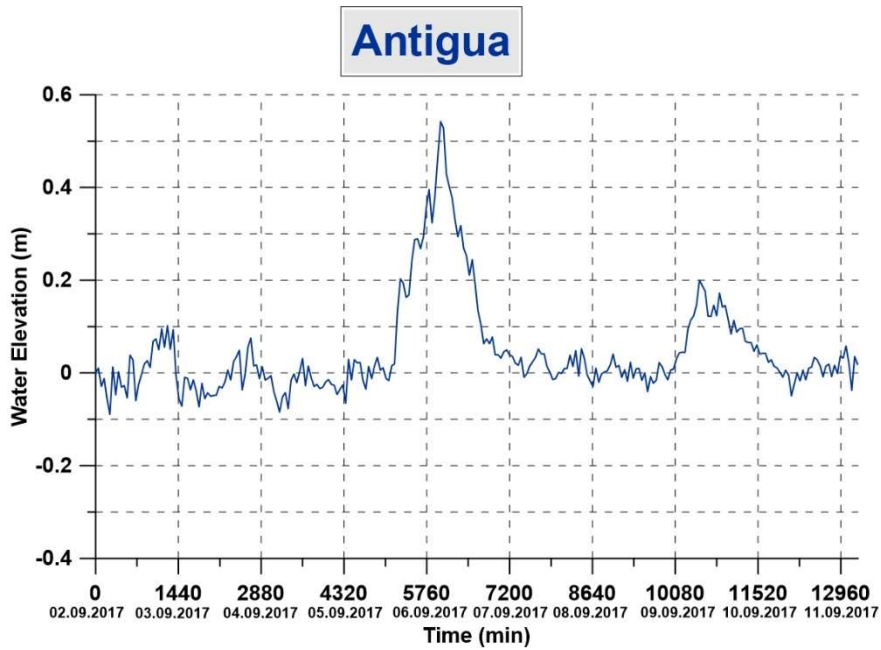


*Figure 4.12. The location of Antigua, Barbuda and Vieques Islands. The horizontal coordinate represents longitude in degree (East) and the vertical coordinate represents for latitude (North)*

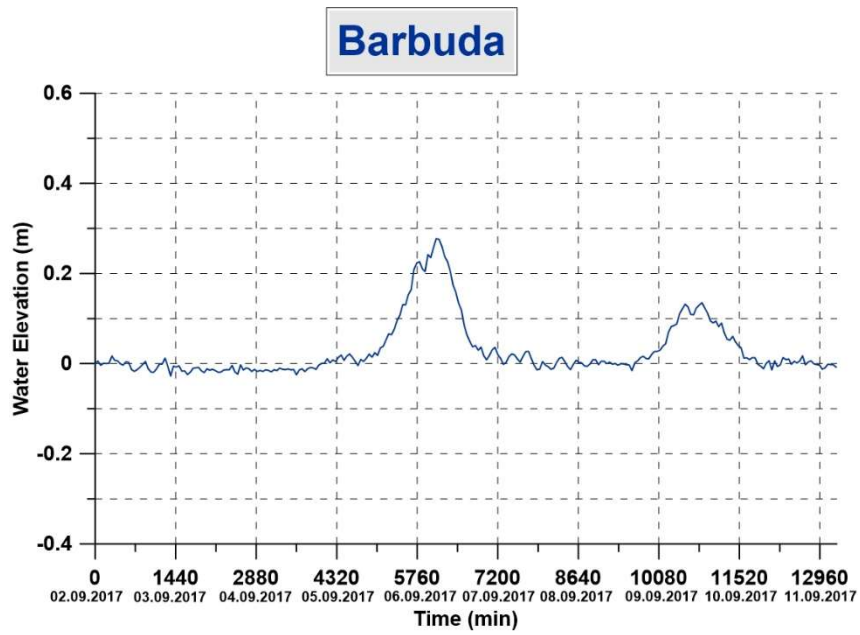
In Table 4.3, the observed and calculated maximum water level, the time of the minimum sea level pressure taken from NOAA's observations and the arrival (or stating) time of the maximum water level increase due to simulation are compared for the selected gauge locations Antigua, Barbuda and Vieques. It should be noted that, in the calculation of the maximum water level change, only long wave generation due to atmospheric pressure and wind values during simulation period (02.09.2017-11.06.2017) are considered. However, the observed wave level values taken from NOAA's land stations include other wave components such as wave set up, wave run up and tide. On the contrary to the difference between observed and calculated maximum water level values, the time of the minimum sea level pressure taken from NOAA's observations and the arrival (or stating) time of the maximum water level increase due to simulation are close. In addition to that, in Figure 4.13, the water elevations for selected points are plotted with respect to time in minute and days.

Table 4.3. The comparison of the simulation results and observed values for Antigua, Barbuda and Vieques Islands

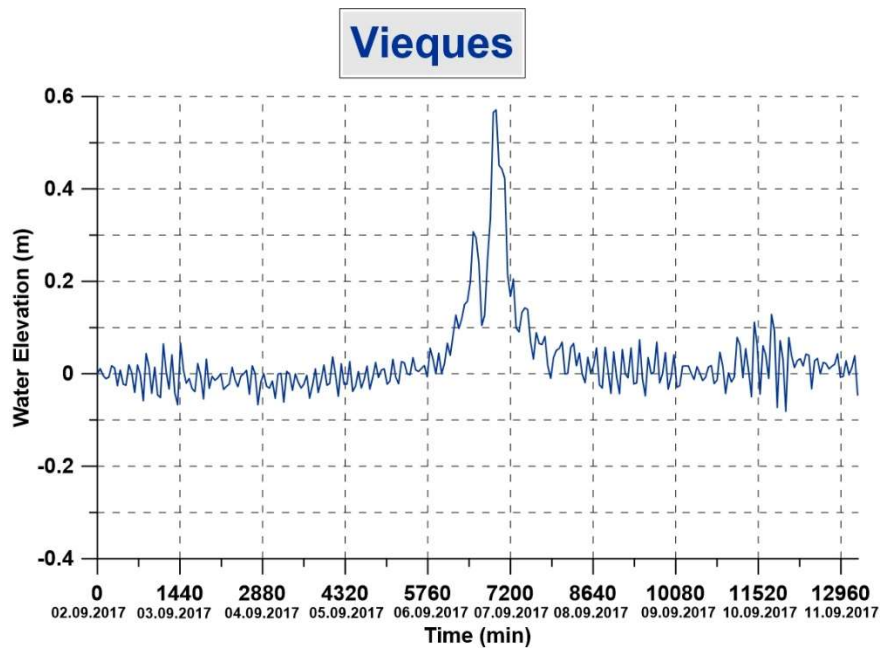
Name	Calculated Max. Water Level (m)	Observed Max. Water Level (m)	Calculated Date of Max. Water Level (date/time)	Observed Min. Sea Level Pressure (date/time)
Antigua	0.53	2.4	06.09/04:48	06/05:36
Barbuda	0.27	2.4	06.06/04:43	06/05:36
Vieques	0.55	0.4	06.09/19:50	06/20:06



(a)



(b)



(c)

Figure 4.13. The numerical model results for a) Antigua, a) Barbuda and c) Vieques

It should be noted that, the computed water level during simulations covers only the water level change due to pressure and wind effects. The measured or observed water levels include the water level change by pressure and wind fields and i) setup by wind forcing, ii) wave setup iii) other physical conditions. Therefore, the measured values are higher than the computed values. However, best fit of the occurrence time of the maximum water level at all stations are obtained between observed data and simulation results. Besides, the possible error in measurement of the pressure and wind data with 1-hour time period (data taken from CFSR) can lead to the water level rise lower than expected.

#### **4.3.2. Application to September 16-30, 2017 Cyclone Maria event**

By 12 September, a well-defined atmospheric circulation developed and became a tropical depression that centered in the east of Barbados Island. In Figure 4.14, the path of the hurricane is shown.

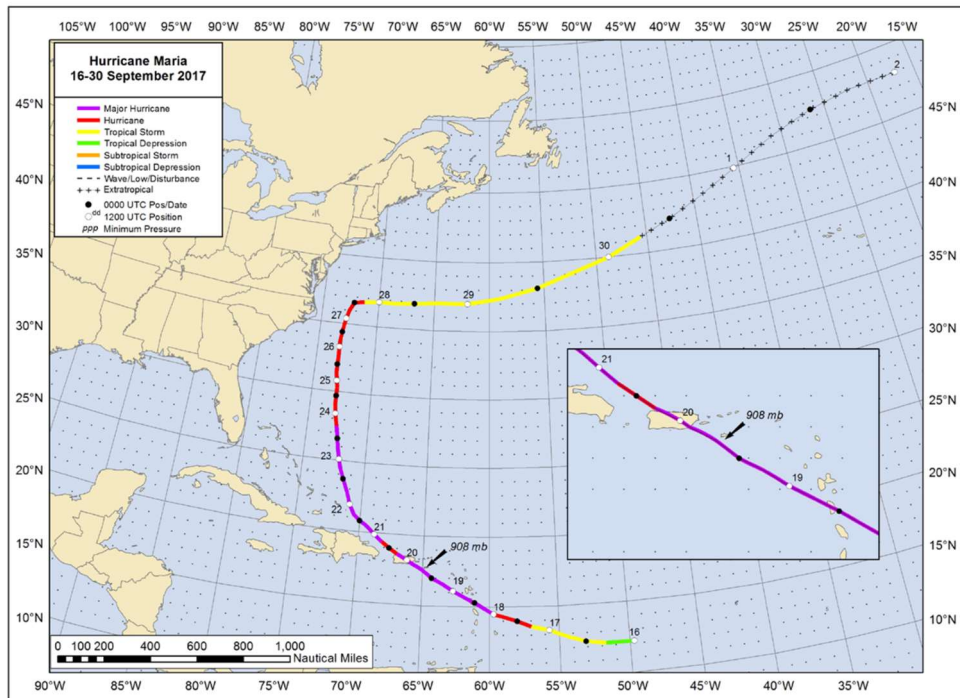


Figure 4.14. The path of Hurricane Maria, 16–30 September 2017, National Hurricane Center, Hurricane Maria Report, 2017).

Maria made landfall over the island of Dominica as a category 5 hurricane on the Saffir-Simpson Hurricane Wind Scale and over Puerto Rico as category 4 hurricane.

According to surface wind estimations done by NHC, on 20 September, the estimated minimum central pressure was 908 mb at 03:13 UTC (Figure 4.15). The maximum wind velocity of the Maria is estimated around 150 kt (77 m/s) (Figure 4.16).

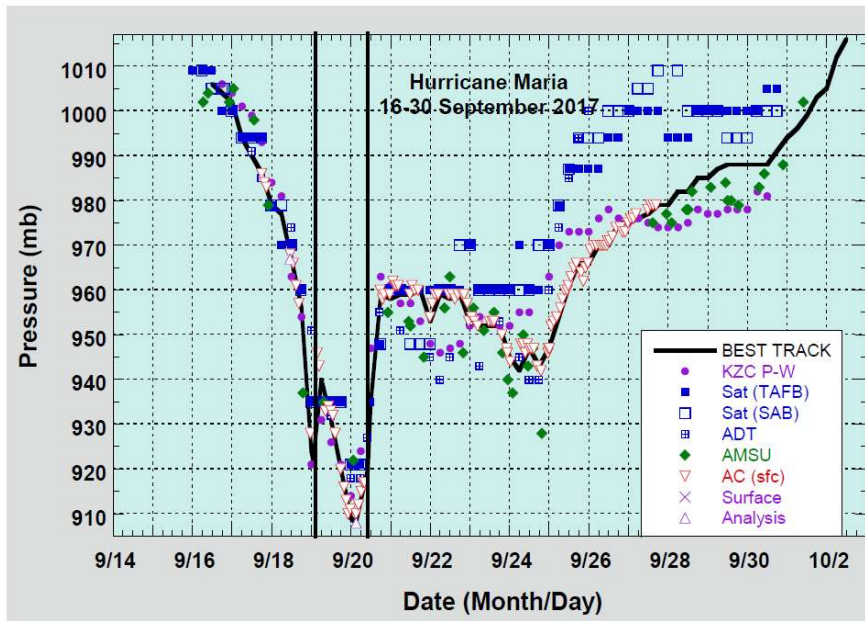


Figure 4.15. Pressure observations and central pressure curve for Hurricane Maria, 16–30 September 2017, National Hurricane Center, Hurricane Maria Report, 2017).

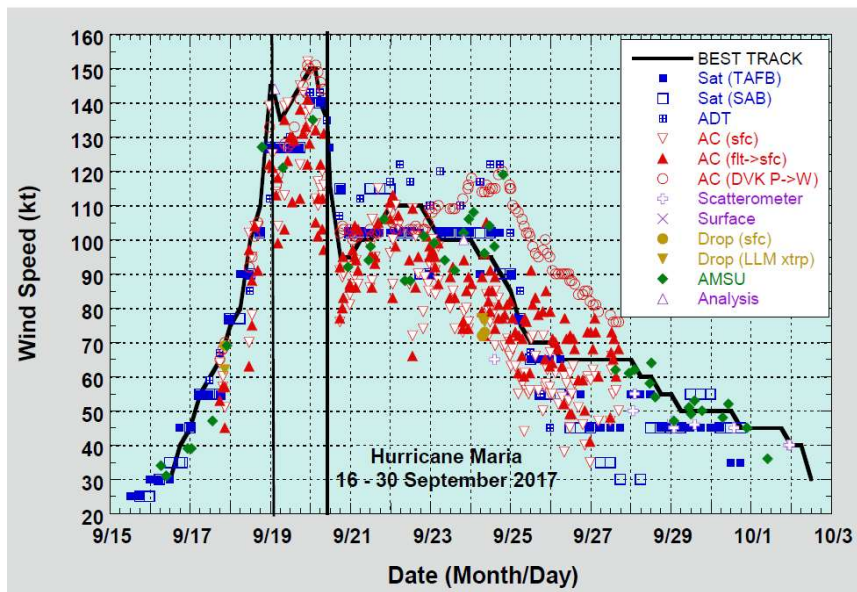


Figure 4.16. Wind speed observations and maximum sustained surface wind speed curve for Hurricane Maria, 16–30 September 2017, National Hurricane Center, Hurricane Maria Report, 2017).

Maria caused around 98 direct deaths with unknown number of indirect deaths in Dominica Guadeloupe and Puerto Rico (National Hurricane Center, Hurricane Maria Report, 2017). The aftermath of the hurricane events for Dominica and Puerto Rico is shown in the Figures 4.17 and 4.18.



*Figure 4.17. Maria's damage in Dominica, National Hurricane Center, Hurricane Maria Report, 2017).*



*Figure 4.18. Maria's damage in Puerto Rico, National Hurricane Center, Hurricane Maria Report, 2017).*

The storm surge generated by Hurricane Maria effected Caribbean Islands, Puerto Rico, the U.S. Virgin Islands. According to field surveys, the measured run ups were range from 1.0 to 3.7 m. The maximum observed run up was at the southern tip of Dominica. The largest measured run ups were generally along the west coast of the southern half of Dominica Island and consistently decreased northwards (Heidarzadeh et. al., 2018).

The tide gauge records from the stations in several regions are studied by Heidarzadeh, Teeuw, Day, Solana (2018) for the period from 13 to 24 of September, 2017 with 1 min record interval. The locations of tide gauges are shown in the Figure 4.19 below.

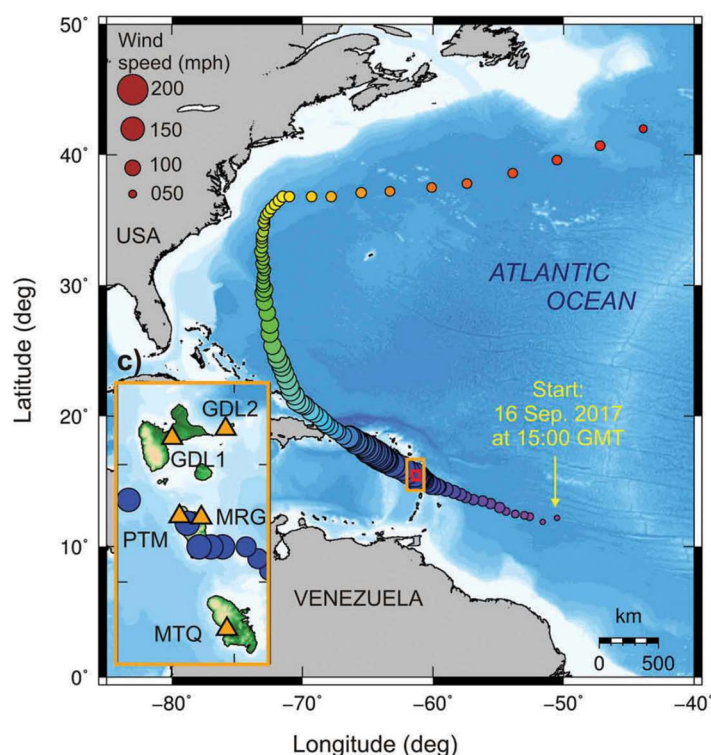


Figure 4.19. The path of Hurricane Maria, the data obtained from the NHC (<https://www.nhc.noaa.gov/>) and tide gauge stations (triangles) used in Heidarzadeh et. al., 2018 are shown with name abbreviations: GDL1, Pointe à Pitre (Guadeloupe)

The selected bathymetry for the numerical model of the storm surge level during Hurricane Maria event is same with the Hurricane Irma. The detailed information about domains are given in the Table 4.2. Also, the coarse and nested bathymetries are shown in the Figure 4.10. The pressure and wind fields are inputted in the duration of 5 days between 16.09.28017-21.09.2017.

Mean sea level pressure data and wind data with 10 m high above the sea level are taken from CFSR (Climate Forecast System Reanalysis), with  $0.50^{\circ} \times 0.50^{\circ}$  (in degree) grid size and 1 hr time period. The pressure and wind distributions on September 20, 2017 at 03:00 UTC taken from CFSR are given in the Appendix Figure A2 as an example.

In the Figure 4.20, the calculated result of the distribution of maximum water elevations during the hurricane event (16.09.2017-21.09.2017) is compared with the path of Hurricane Maria taken from National Hurricane Center, Hurricane Maria Report (2017). The distribution of the maximum water elevations forms a path that is matched with the path of the Hurricane Irma provided from NHC. As a result, the simulation shows that the numerical results can catch the observed best track positions for Hurricane Maria.

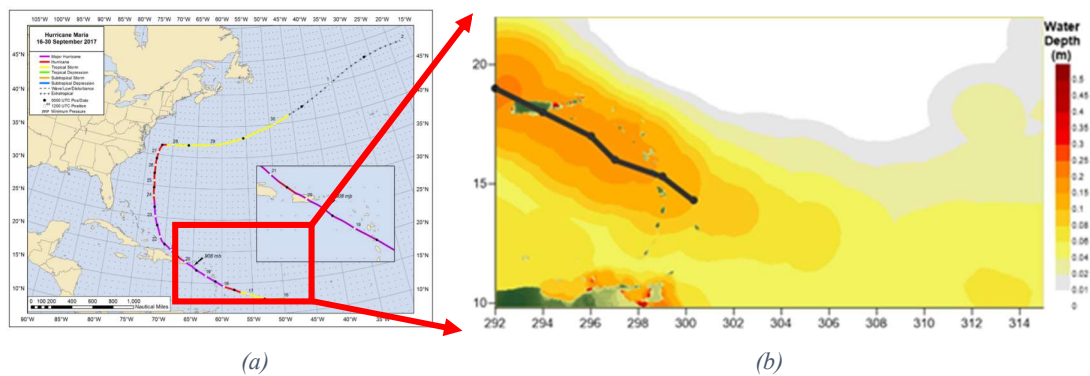


Figure 4.20. a) The path of the Hurricane Maria taken from NHC, Hurricane Maria Report, 2017. b) Distribution of maximum water level due to atmospheric pressure and wind during Maria and the path of the storm taken by NHC Hurricane Maria Report (black line). The horizontal coordinate represents longitude in degree (East) and the vertical coordinate represents for latitude (North)

In Table 4.4, the maximum water level and arrival date maximum water level found from simulation are compared with the de-tided one-hour averaged waveforms given by Heidarzadeh et. al. (2018) for the selected gauge locations for GDL1, Pointe à Pitre (Guadeloupe); GDL2, La Desirade Island (Guadeloupe); PTM, Portsmouth (Dominica); MRG, Marigot (Dominica); MTQ, Martinique (Fort de France). The numerical results are lower than the observed water levels. In Figure 4.21, the water elevation changes that are taken from Heidarzadeh et. al. (2018) during Hurricane Maria event are shown for 5 different gauge points. The calculated arrival time of the maximum water levels for the 5 gauge locations given in the Table 4.4 are close with the time of the maximum water level shown in the Figure 4.21. However, the maximum water level is lower than the observed values. In addition to that, in Figure 4.22, the water elevation change for selected gauge points during the period of the numerical simulation are plotted.

Table 4.4. The maximum water levels and their arrival time for GDL-2, GDL-1, MRG, PTM and MTQ.

Name	Calculated Max. Water Level (m)	Observed One-hour Averaged Waveforms (m)	Arrival Date of Max Wave (date/time)
GDL-2	0.18	0.60	19/03:52
GDL-1	0.3	0.52	19/03:04
MRG	0.218	0.75	19/11:40
PTM	0.164	-	19/06:11
MTQ	0.25	0.25	19/03:34

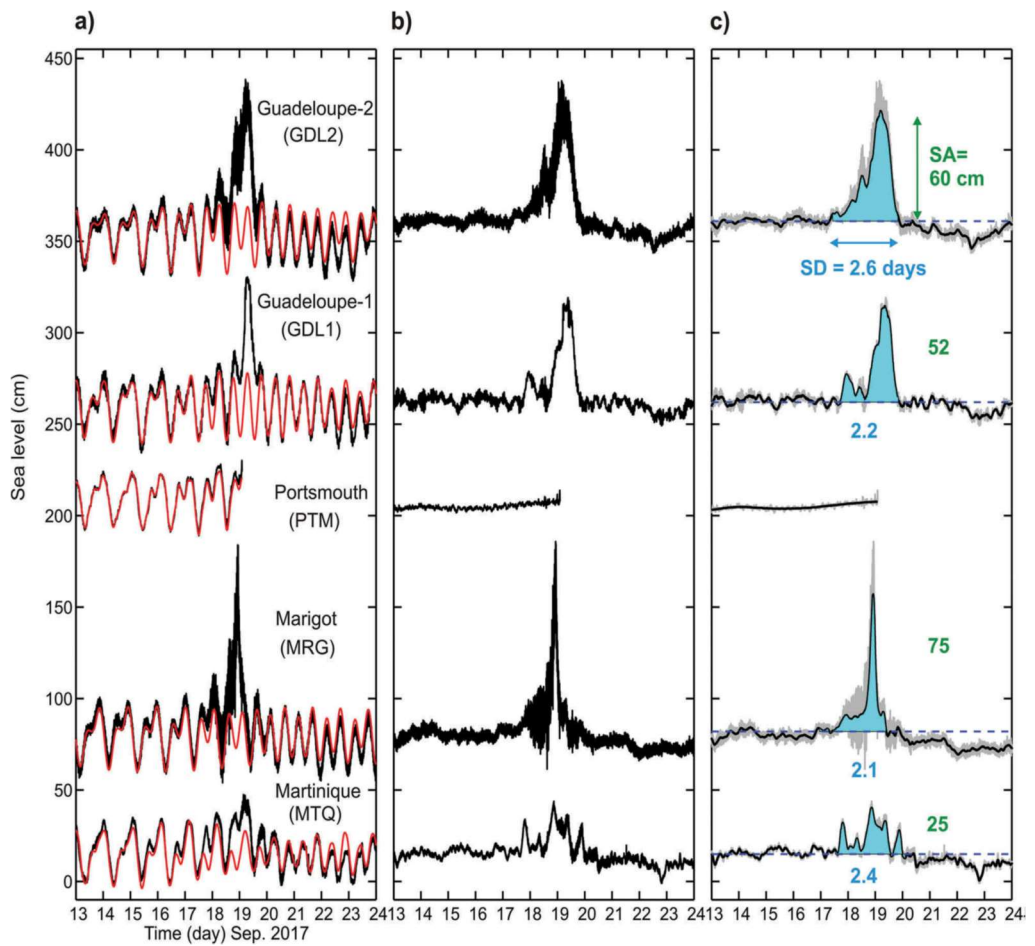
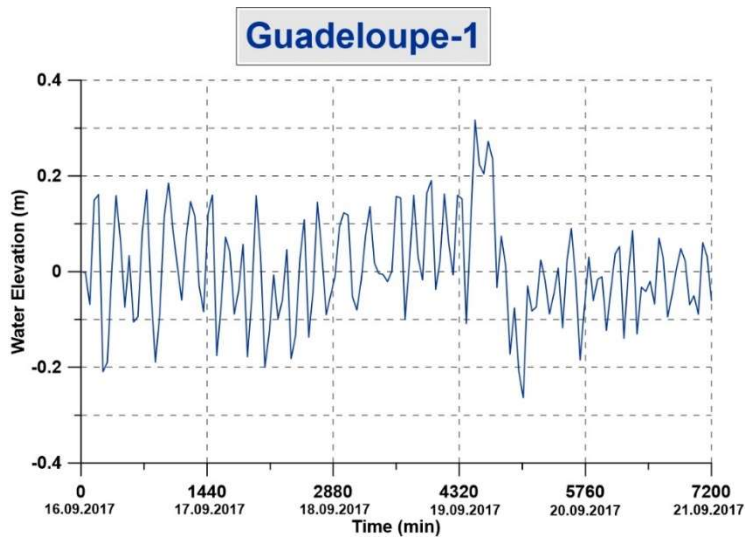
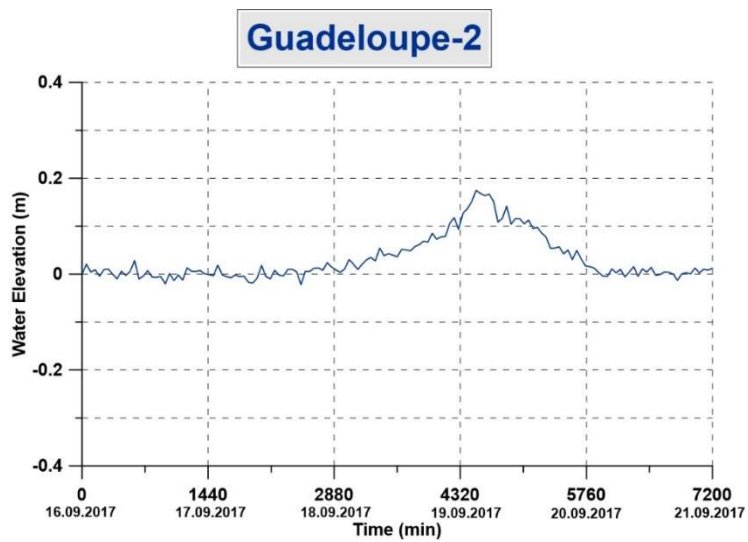


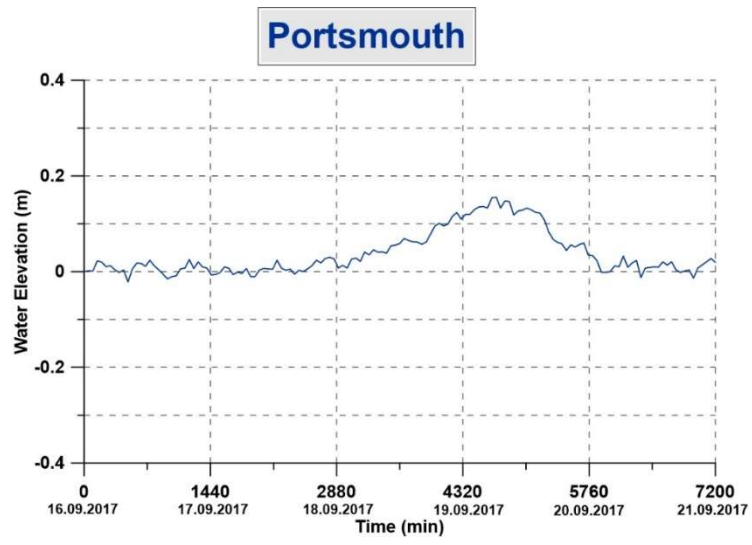
Figure 4.21. a) The original tide gauge records, b) The de-tided tide gauge waveforms, c) The one-hour averaged waveforms representing the storm surge amplitudes (Heidarzadeh et al., 2018)



(a)



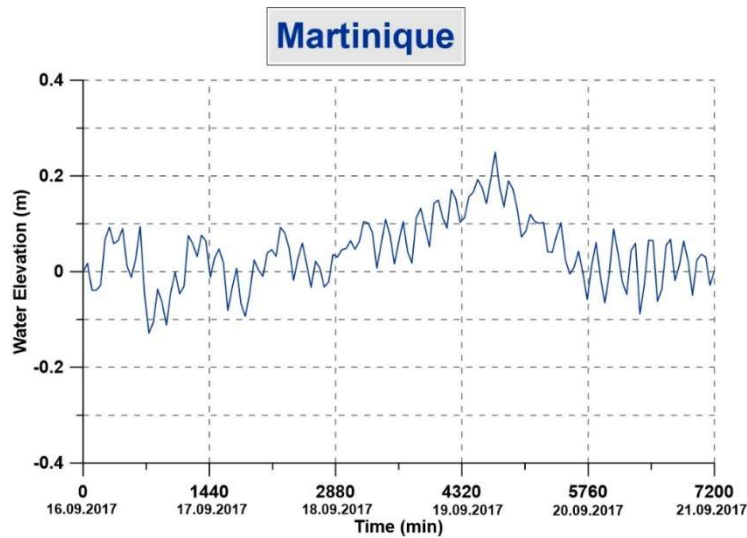
(b)



(c)



(d)



(e)

Figure 4.22. The numerical model results for a) GDL1, Pointe à Pitre (Guadeloupe); b) GDL2, La Desirade Island (Guadeloupe); c) PTM, Portsmouth (Dominica); d) MRG, Marigot (Dominica); e) MTQ, Martinique (Fort de France)

The tide gauge records, the de-tided tide gauge waveforms and the one-hour averaged waveforms representing the storm surge amplitudes the water elevations for selected points that are taken from Heidarzadeh et. al. (2018) compared with the NAMI DANCE numerical results for storm surge level during Hurricane Maria. The time of the maximum water elevations are matched with the selected gauge points. It should be noted that, as it is mentioned in Hurricane Irma case, the reason of the difference between the sea level elevation from tide gauges and numerical modeling can be due to excluding of several wave components that is effective in the sea level change such as wave setup, wave runup and tide (see Table 3.1). Besides, the possible error in measurement of the pressure and wind data with 1-hour time period (data taken from CFSR) can lead to the water level rise lower than expected.

### 4.3.3. Application to 16-25 January, 2018 Aegean Event

A storm event was observed over Aegean Sea between 16-25 January, 2018. The storm was effective in Syros Island and the western and northern coast of Turkey, especially Izmir and Bodrum.

The strong southwest wind that was on Syros on the evening of Wednesday, 17 January, caused large tree drops in central provincial roads without causing accidents or other serious damage (“Bad weather in Syros”,2018). On the other hand, the storm caused flooding and big waves in the Muğla's Bodrum district on 18 January 2018 (Figure 4.23). In Izmir, which is the most effective, the wind speed reached up to 103 km/hr. In Aliğa distirict, a cargo ship dragged ashore (Figure 4.24).

Storm was also effective in Zonguldak. The waves damaged workplaces, cars and fishing boats. In Bozcaada, some ferry services were canceled due to the storm. Storm waves reached Sochi, Russia.



Figure 4.23. The storm caused big waves in Bodrum, Mugla, Turkey (“Bodrum'da sağanak”, 2018)



Figure 4.24. The storm damage in Izmir, Turkey (“İzmir'deki fırtına”, 2018)

For the numerical modeling of the storm a bathymetry with 900 m grid size obtained from GEBCO is selected. Considering the effective time of the storm, run time with 1 hr period between the dates 16.01.2018-24.01.2018 is selected. The detailed information about bathymetry is given in the Table 4.5 below. Also, the bathymetry used for numerical modeling is shown in the Figure 4.25.

Table 4.5. The detailed information about size of bathymetry

Bathymetry	Grid Size (m)	Coordination			
	900	-6E	42E	30N	47.5N

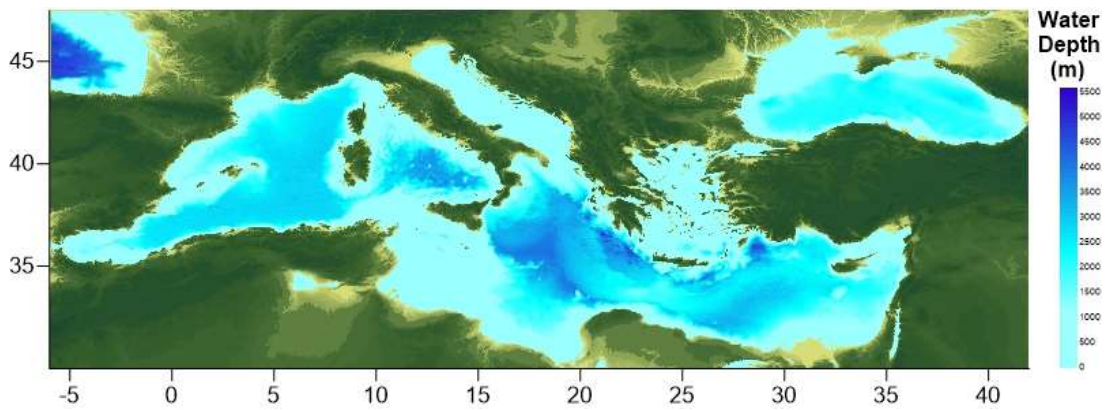


Figure 4.25. The bathymetry used for numerical modeling of the storm.

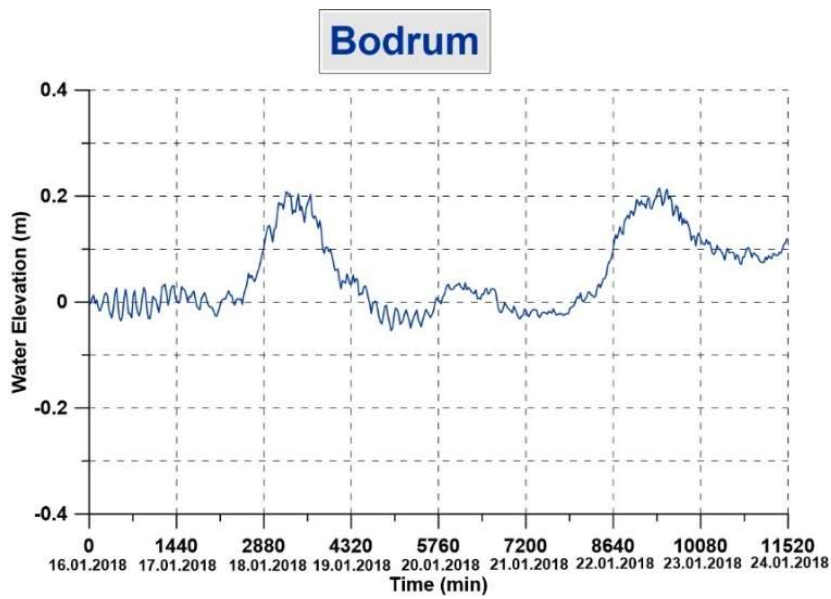
Mean sea level pressure data and wind data with 10 m high above the sea level are taken from JRC, with 1 hr time period between 16.01.2018 and 24.01.2018. The pressure and wind distributions on January 18, 2018 at 12:00 UTC taken from JRC are given in the Appendix Figure A3 as an example. In Table 4.6, the maximum and the minimum water level and starting date of the maximum water level are given for the selected gauge locations for Izmir and Bodrum. The results for the selected Izmir and Bodrum are shown in the Figures 4.26.

Table 4.6. The calculated maximum water level and their arrival time for selected locations Izmir and Bodrum.

<b>Name</b>	<b>Calculated Max. Water Level (m)</b>	<b>Arrival Date of Max Water Level (date/time)</b>
Izmir	0.32	18/07:25
Bodrum	0.22	22/12:36



(a)



(b)

Figure 4.26. The sea level elevation during storm in a) Izmir and b) Bodrum, Turkey

According to the news the storm was effective in 18 January 2018. The simulation results for Izmir and Bodrum show water level rising between 18-19 January. The second water level rise can be reason of a second storm which was effective in the selected locations. However, since this assumption is based on news, further investigations are needed.

#### **4.3.4. Application to September 29-October 01, 2018 Medicane Event**

The tropical storm on late September 27 started off the coast of the Libya and affected the Mediterranean–Aegean Sea region until 01 October 2018. After reaching the Aegean Sea by passing through the South of Crete and Peloponnese Peninsula, the tropical storm turned to the north of the Aegean Sea on 30 September 2018. It also affected Sicily and Malta Island. It has caused damage to the coasts in various parts of the Peloponnese Peninsula of Greece. In the Aegean coast of Turkey, which is slightly less effective storm, it has caused strong winds and heavy rains. According to the news, in Akyaka, sea level recedes 0.2 m (Figure 4.27).



*Figure 4.27. Sea Recedes at Akyaka, Turkey, (Ward, L., 2018).*

For the numerical modeling of the storm, same bathymetry is used. The detailed information about bathymetry is given in the Table 4.7. Also, the domain is shown in the Figure 4.28.

Table 4.7. The information of the model domain

Bathymetry	Grid Size (m)	Coordination			
	900	-3E	34E	31N	47.5N

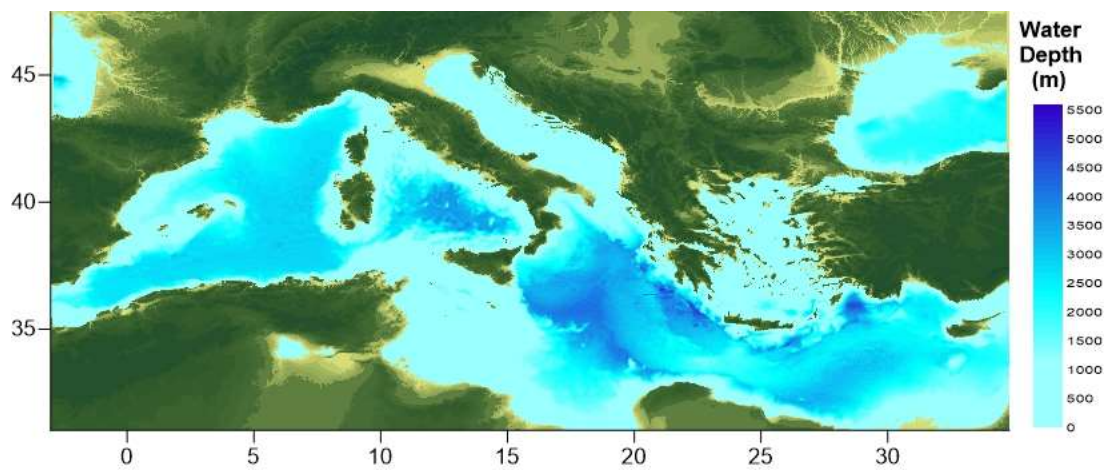


Figure 4.28. The bathymetry used for numerical modeling of the storm.

Mean sea level pressure data and wind data with 10 m high above the sea level are taken from CFSR (Climate Forecast System Reanalysis), with 0.50x0.50 grid size and 6 hr time period. The pressure and wind distributions on September 29, 2018 at 01:00 UTC taken from CFSR are given in the Appendix Figure A4 as an example. In Table 4.8, the maximum and the minimum water level change and arrival date of the maximum water level are given for the selected gauge locations for Izmir and Bodrum. Also, the results for the selected areas are shown in the Figure 4.29.

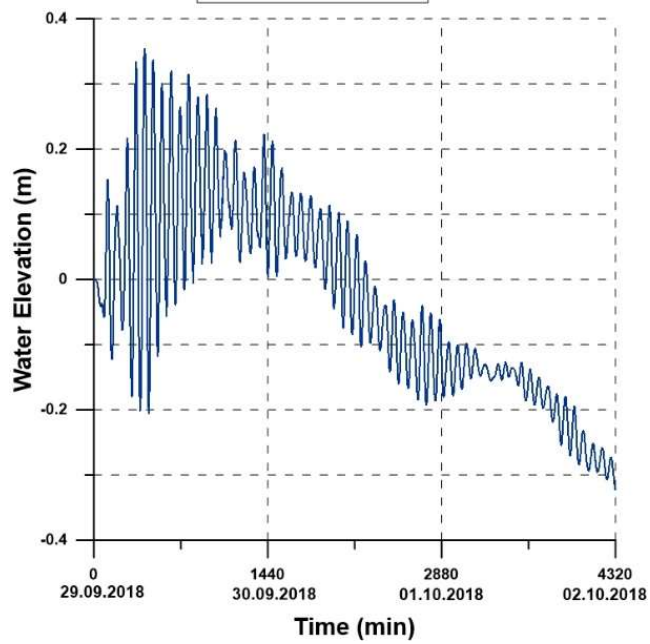
Table 4.8. The calculated max. and min. water level change and arrival time of max. water level for Stazzo, Nea Kios and Akyaka.

Name	Calculated Max. Water Level (m)	Calculated Min. Water Level (m)	Arrival Date of Max Water Level (date/time)
Stazzo	0.086	-0.268	556
Nea Kios	0.354	-0.32255	419
Akyaka	0.169	-0.335	794.75

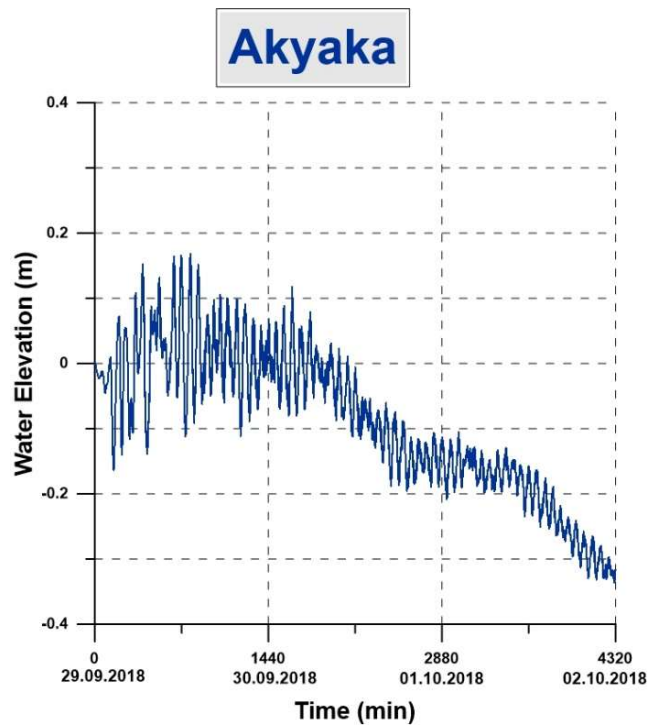


(a)

# Nea Kios



(b)



(c)

Figure 4.29. The numerical model results for a) Stazzo, Sicily; b) Nea Kios, Greece; c) Akyaka, Turkey

According to the news, in Akyaka region, sea level decrease about 20 cm. The results for the Akyaka provided that the tropical cyclone cause decrease. However, since, the pressure and wind data is not sufficient to catch the Medicane and the water level assumption is based on news, further investigations are needed.



## CHAPTER 5

### CONCLUSION

Storm surge is tsunami-like long wave that generated during storm events like cyclones. It can be observed all over the world and damages coastal areas and causes loss of lives. Even though, the generation mechanism is different, storm surge waves show similarities with tsunami waves as they are long period waves. Water level change during the storm surge are caused by the large scale atmospheric pressure differences. The rising of the water level is associated with low pressure disturbance systems, as the decrease in the water level is associated with high pressure disturbance systems.

The aim of this study was to compute the long wave elevation and propagation caused by moving atmospheric pressure difference and strong wind fields occurred during storm events. For this purpose, the numerical model NAMI DANCE is used.

In this thesis, particularly water level increase and decrease due to moving atmospheric forcing during storms and tropical cyclones are studied. First, different approaches associated with modeling of meteorological origin long waves are investigated. The atmospheric pressure source parameter and wind source parameters for x and y direction are inserted into Nonlinear Shallow Water Equations (long wave equations). Hence, the storm surge phenomena implemented in the tsunami numerical model NAMI DANCE, which have already solved the nonlinear form of depth averaged shallow water equations for tsunamis.

In the verification process, the aim was to ensure that numerical model can compute the water surface elevations due to the effect of static circular atmospheric pressure disturbances for regular shaped flat bathymetry. The model was tested for cyclone and anticyclone cases. For this reason, the circular shaped low and high static pressure disturbance applied to flat bathymetry. The computed results for the two cases are in agreement with the analytical results.

In the validation process, the aim was to ensure that the numerical model can provide an accurate representation of the real world storm and cyclone events. For this reason, the model is applied to four different recent storm events occurred in Caribbean and Mediterranean regions.

In the NAMI DANCE model, the water level change during storm events covers only the long term water level change (long waves generated by pressure and wind fields). However, the measured or observed water levels often include the water level change by pressure and wind fields and also other physical conditions such as setup by wind forcing, wave setup and tide. These physical conditions are effective during storm events and can further increase or decrease water level. Moreover, the possible error in measurement of the pressure and wind data can also affect the observed water level change. As a results, the numerical model values are lower than the observed values in general.

The results of the simulations indicate that the occurrence time of the maximum water level are in agreement with the observed time values. In addition to that, the numerical results provided from Hurricane Irma and Maria events shows that the model can also indicate the path of the storm accurately.

As a results, the simulations for four storm events point out that the numerical model can:

- Show the path of the storm,
- Indicate the increasing or decreasing in the long time water level change due to only moving atmospheric pressure and wind,
- Detect the occurrence time of the maximum water elevations,
- Detect the duration of storm surge.

### **Future Recommendations:**

The test studies are conducted on both the regular shaped bathymetries and real cases to clarify the fundamental concepts related to the storm surge. In order to obtain more accurate results, high spatial and temporal resolution for atmospheric pressure should be used. In addition to that, during the cyclone modeling calculations, as it is indicated, some of the physical processes of ocean waves are not included. To achieve more accurate results with the wave gauges some of the physical processes like wave setup, tides, wave shoaling and wave refraction can be added to the numerical model.



## REFERENCES

Alimov, V. V. (2005). Integrated modeling of storm surges during hurricanes Isabel, Charley, and Frances. PhD. University of Florida.

Aydın, C.C. (2016). Surge and coastal inundation study of September 2014 storm in Giresun, Black Sea, MSc Thesis, METU

Bad weather in Syros: The winds threw trees, umbrellas, awnings and signs, (2018) Retrieved from <https://cyclades24.gr/2018/01/kakokairia-syros-dentra-ompreles-pinakides/>

Blumberg, A. F. and Mellor, G. L. (1987). A description of a three-dimensional coastal ocean circulation model. Three-Dimensional Coastal Ocean Models, edited by N. Heaps, American Geophysical Union.

Bodrum'da sağanak ve fırtına etkili oluyor,(2018) Retrieved from <http://beyazgazete.com/video/webtv/guncel-1/bodrum-da-saganak-ve-firtina-etkili-oluyor-mugla-482103.html>

Cavicchia, L., von Storch, H. and Gualdi, S.: A long-term climatology of medicanes, Clim. Dynam., doi:10.1007/s00382-013-1893-7, online first, 2013

Charnock, H. (1955) Wind Stress on a Water Surface. Quarterly Journal of the Royal Meteorological Society, 81, 639-640. <http://dx.doi.org/10.1002/qj.4970813502>

Chao An, Philip L-F. Liu, and Seung Nam Seo. "Large-scale edge waves generated by a moving atmospheric pressure" Theor. Appl. Mech. Lett., vol. 2, no. 4, 2012. doi:10.1063/2.1204201

COMCOT Manual (2009). Developed by Xiaoming Wang, Liu, P. Y.-S. Cho, S.-B.Woo. USER MANUAL FOR COMCOT VERSION 1.7 (FIRST DRAFT).

<http://citeseerx.ist.psu.edu/viewdoc/download?doi=10.1.1.512.84&rep=rep1&type=pdf>

Ergin, A., 2010. Coastal Engineering, METU Press, Ankara, Turkey.

Franchello, G., and Krausmann, E. (2008). HyFlux2: a numerical model for the impact assessment of severe inundation scenario to chemical facilities and downstream environment. EUR 23354 EN – 2008, ISSN 1018-5593.

Garratt, J. R. (1977). Review of drag coefficients over oceans and continents. Monthly Weather Review, 105:915-929.

Heidarzadeh, M., Teeuw, R., Day S., and Solana, C. (2018). Storm wave runups and sea level variations for the September 2017 Hurricane Maria along the coast of Dominica, eastern Caribbean Sea: evidence from field surveys and sea-level data analysis, Coastal Engineering Journal, 60:3, 371-384, DOI: 10.1080/21664250.2018.1546269

Hibiya, T., & Kajiura, K. (1982). Origin of the Abiki phenomenon (a kind of seiche) in Nagasaki Bay. Journal of the Oceanographical Society of Japan, 38(3), 172-182.

Higaki, M., Hayashibara, H., and Nozaki, F. (2009). 25-38. Retrieved 2011, from JMA, Technical Review, No. 11: <http://www.jma.go.jp/jma/jma-eng/jma-center/rsmc-hp-pub-eg/techrev/text11.pdf>

İzmir'deki fırtına, (2018) Retrieved from <http://www.haber7.com/izmir/2527783-izmirdeki-firtina>

Jansa, A., Monserrat, S., and Gomis, D.: The rissaga of 15 June 2006 in Ciutadella (Menorca), a meteorological tsunami, Adv. Geosci., 12, 1-4, <https://doi.org/10.5194/adgeo-12-1-2007>, 2007.

Jelesnianski, C. P., Chen, J., and Shafer, A. W. (1992). SLOSH: Sea, Lake, and Overland Surges from Hurricanes. Technical Report of National Weather Service, Silver Spring, MD, 48:71.

Kakinuma, T., & Fukita, K. (2012). A Numerical Study on Long-Wave Generation Due to Atmospheric-Pressure Variation. *Coastal Engineering Proceedings*, 1(33), currents.17. doi:<https://doi.org/10.9753/icce.v33.currents.17>

Lionello, P., “Extreme storm surges in the gulf of Venice: present and future climate,” in *Venice and Its Lagoon, State of Knowledge*, C. Fletcher and T. Spencer, Eds., pp. 59–65, 2005.

Lionello, P., Sanna, A., Elvini, E., and Mufato, R., “A data assimilation procedure for operational prediction of storm surge in the northern Adriatic Sea,” *Continental Shelf Research*, vol. 26, no. 4, pp. 539–553, 2006.

Luetlich, R., Westerink, J. J., and Scheffner, N. W. (1992). ADCIRC: an advanced three-dimensional circulation model for shelves coasts and estuaries, report 1: theory and methodology of ADCIRC-2DDI and ADCIRC-3DL. Dredging Research Program Technical Report DRP-92-6, U.S. Army Engineers Waterways Experiment Station, Vicksburg, MS, page 137.

Liu, P. L. F. and Dalrymple, R. A. (1978). Bottom frictional stresses and longshore currents due to waves with large angles of incidence. *J. of Marine Res.*, 36:357-375.

Mel R., (2013). Future developments in surge forecast: probabilistic forecast and future surge statistic (Doctoral dissertation). University of Padova.

Metin A., D., (2016). Long waves generation and coastal amplification due to atmospheric pressure disturbances MSc Thesis, METU

Monserrat, S., Ibbetson, A., & Thorpe, A. J. (1991). Atmospheric gravity waves and the ‘rissaga’ phenomenon. *Quarterly Journal of the Royal Meteorological Society*, 117(499), 553-570.

Monserrat, S., Vilibic, I., and Rabinovich, A. B.: Meteotsunamis: atmospherically induced destructive ocean waves in the tsunami frequency band, *Nat. Hazards Earth Syst. Sci.*, 6, 1035–1051, 2006

NAMI DANCE Manual (2010). Developed by Zaytsev, C., Yalciner, Pelinovsky, Kurkin. Tsunami Simulation/Visualization Code NAMI DANCE versions 4.9. <http://www.namidance.ce.metu.edu.tr>

National Hurricane Center, Tropical Cyclone Report: Hurricane Irma Report, 2017

National Hurricane Center, Tropical Cyclone Report: Hurricane Maria Report, 2017

NOAA, Historical Hurricane Tracks data base. Retrieved from <https://www.coast.noaa.gov/hurricanes/>

Powell, M. D., Vickery, P. J., and Reinhold, T. A., 2003. Reduced drag coefficient for high wind speeds in tropical cyclones, *Nature*, 422, 279–283, doi: 10.1038/nature 01481.

Pugh, D. (2004). *Changing sea levels: effects of tides, weather, and climate*. Cambridge Univ Pr.

Rabinovich, A. B. and Monserrat, S.: Generation of meteorological tsunamis (large amplitude seiches) near the Balearic and Kuril Islands, *Nat. Hazards*, 18(1), 27–55, 1998.

Romero, R., and K. Emanuel, 2013: Medicane risk in a changing climate. *J. Geophys. Res. Atmos.*, 118, 5992–6001, doi:10.1002/jgrd.50475.

Šepić, J., Vilibić, I., Rabinovich, A. B., & Monserrat, S. (2015). Widespread tsunami-like waves of 23-27 June in the Mediterranean and Black Seas generated by high-altitude atmospheric forcing. *Scientific reports*, 5.

Schlesinger, S. (1979). Terminology for model credibility, *Simulation*, vol. 32, no. 3, pp. 103-104.

Sorensen, R., M., (2006). Basic Coastal Engineering, Springer Science & Business Media.

Taylor, G. I., (1916). Skin friction of the wind on the Earth's surface. Proc. Roy. Soc. London, A92, 196-199

Velioglu, D., (2017). Advanced Two- and Three-Dimensional Tsunami Models: Benchmarking and Validation (Doctoral dissertation). Middle East Technical University.

World Meteorological Organization (2011) Guide to storm surge forecasting. Geneva, Switzerland, World Meteorological Organization, 120pp. (WMO-No 1076). <http://hdl.handle.net/11329/393>

Ward, L., (2018). Mediane aftermath in Greece and Turkey severe winds torrential rainfall major flooding and tornadoes. Retrieved from [https://www.fethiyetimes.com/news/44-news/28007\\_medicane-aftermath-in-greece-and-turkey-severe-winds-torrential-rainfall-major-flooding-and-tornadoes.html](https://www.fethiyetimes.com/news/44-news/28007_medicane-aftermath-in-greece-and-turkey-severe-winds-torrential-rainfall-major-flooding-and-tornadoes.html)

Wrobel-Niedzwiecka, I., Drozdowska, V., and Piskozub, J.: Air-sea momentum flux climatologies: A review of drag relation for parameterization choice on wind stress in the North Atlantic and the European Arctic, Ocean Sci. Discuss., <https://doi.org/10.5194/os-2018-61>, 2018.

Yalciner, A. C., Kian, R., Aytore, B., & Zaytsev, A. (2015). Harbors and Tsunami Threat; A case study in the Sea of Marmara. E-proceedings of the 36th IAHR World Congress 28 June – 3 July, 2015, The Hague, the Netherlands

Yalciner, A. C., Ozer, C., Karakus, H., Zaytsev, A. and Guler, I. (2010). Evaluation of Coastal Risk at Selected Sites against Eastern Mediterranean Tsunamis. Proceedings of 32nd International Conference on Coastal Engineering. Shanghai, China.

Yalciner, A. C., Pelinovsky, E., Zaytsev, A., Kurkin, A., Ozer, C., and Karakus, H. (2007a). Modeling and Visualization of Tsunamis: Mediterranean Examples from Tsunami and Nonlinear Waves. (A. Kundu, Ed.) Springer, 2731-2839.

Yalciner, A.C., Suppasri, A., Mas, E., Kalligeris, N., Necmioglu, O., Imamura, F., Ozer, C., Zaitsev, A., Ozel, N.M. and Synolakis, C. (2012). Field Survey on the Coastal Impacts of March 11, 2011 Great East Japan Tsunami. Pure Appl. Geophys.

Yalciner, A.C., Yalciner, B., Annunziato, A., Cabuk, O., Probst P. (2019). Modeling of Storm Surge and Inundation with Respect to Pressure and Wind Fields. The First World Conference on Meteotsunamis, Split, Croatia, 2019

Zaitsev, A., Yalciner, A. C., Pelinovsky, E., Kurkin, A., Ozer, C. and Insel, I. (2008). Tsunamis in Eastern Mediterranean Histories, Possibilities and Realities. Proceedings of 7th International Conference on Coastal and Port Engineering in Developing Countries. Dubai, USA.

Zhang, M. Y. and Li, Y. S. (1996). The synchronous coupling of a third-generation wave model and a two-dimensional storm surge model. Ocean Eng., 23:533-543.

## APPENDIX

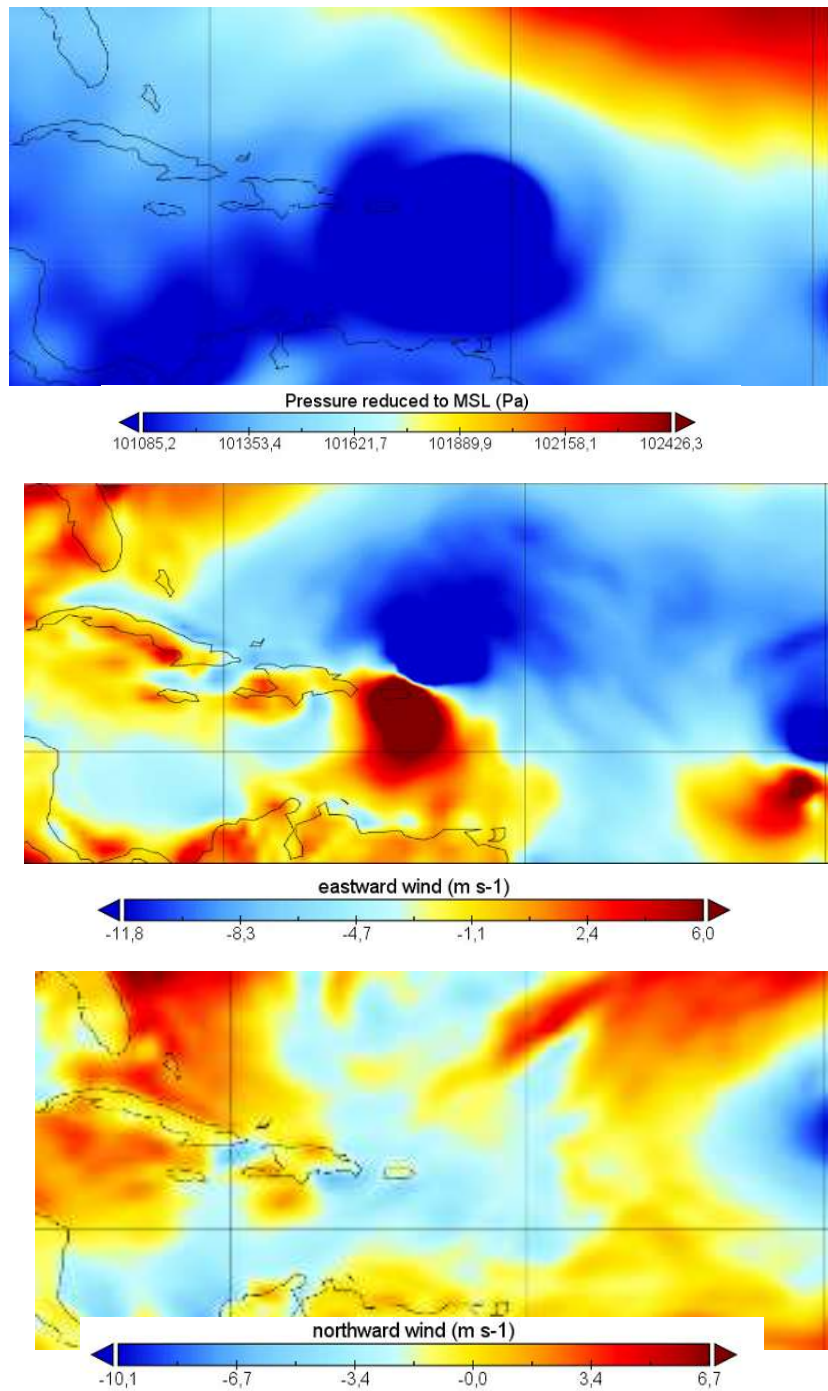


*Figure A.1.* The atmospheric pressure, eastward wind and northward wind data of Hurricane Irma taken from CFSR on September 06, 2017 at 05:00 UTC

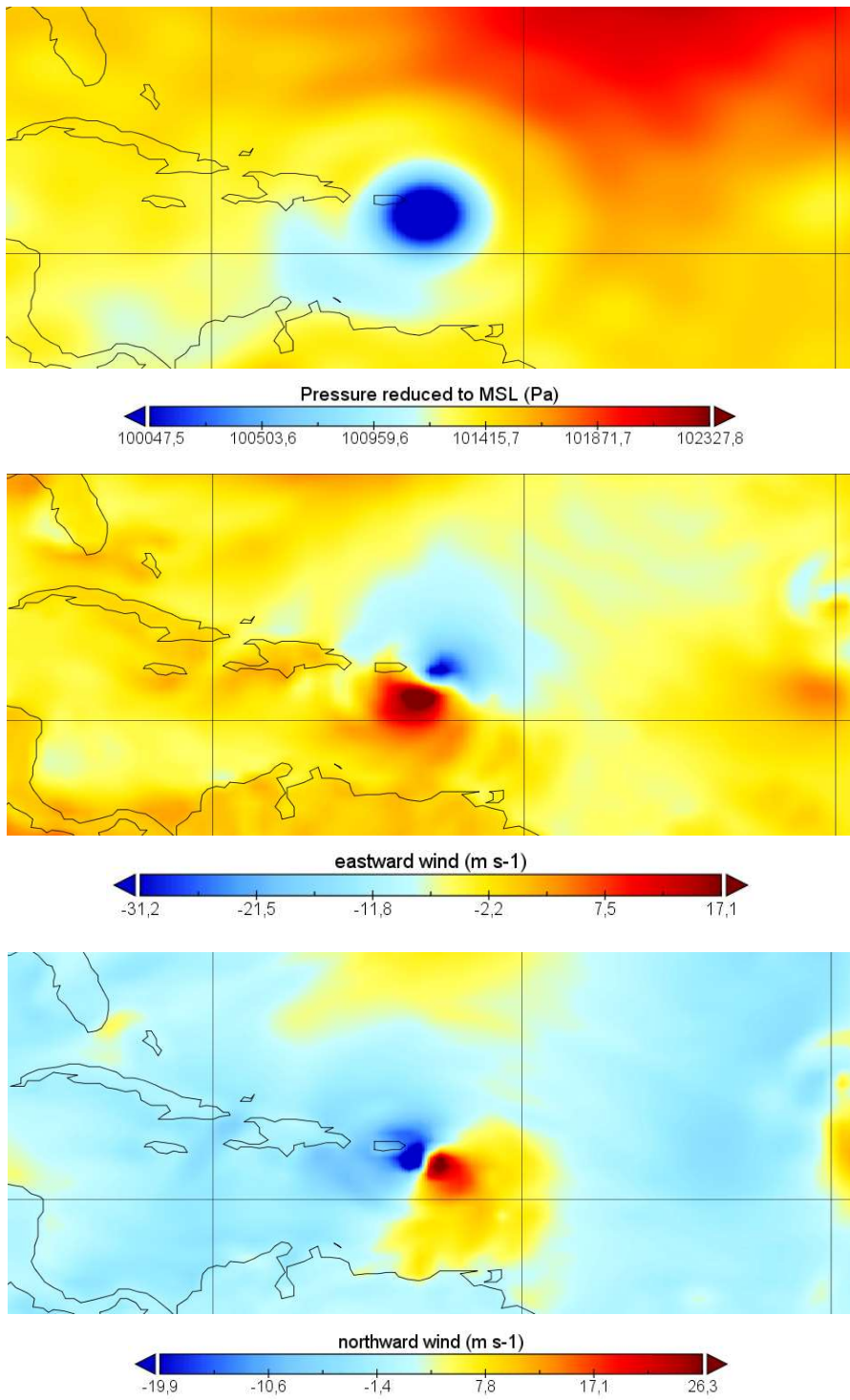


*Figure A.2.* The atmospheric pressure, eastward wind and northward wind data of Hurricane Irma taken from CFSR on September 20, 2017 at 03:00 UTC.

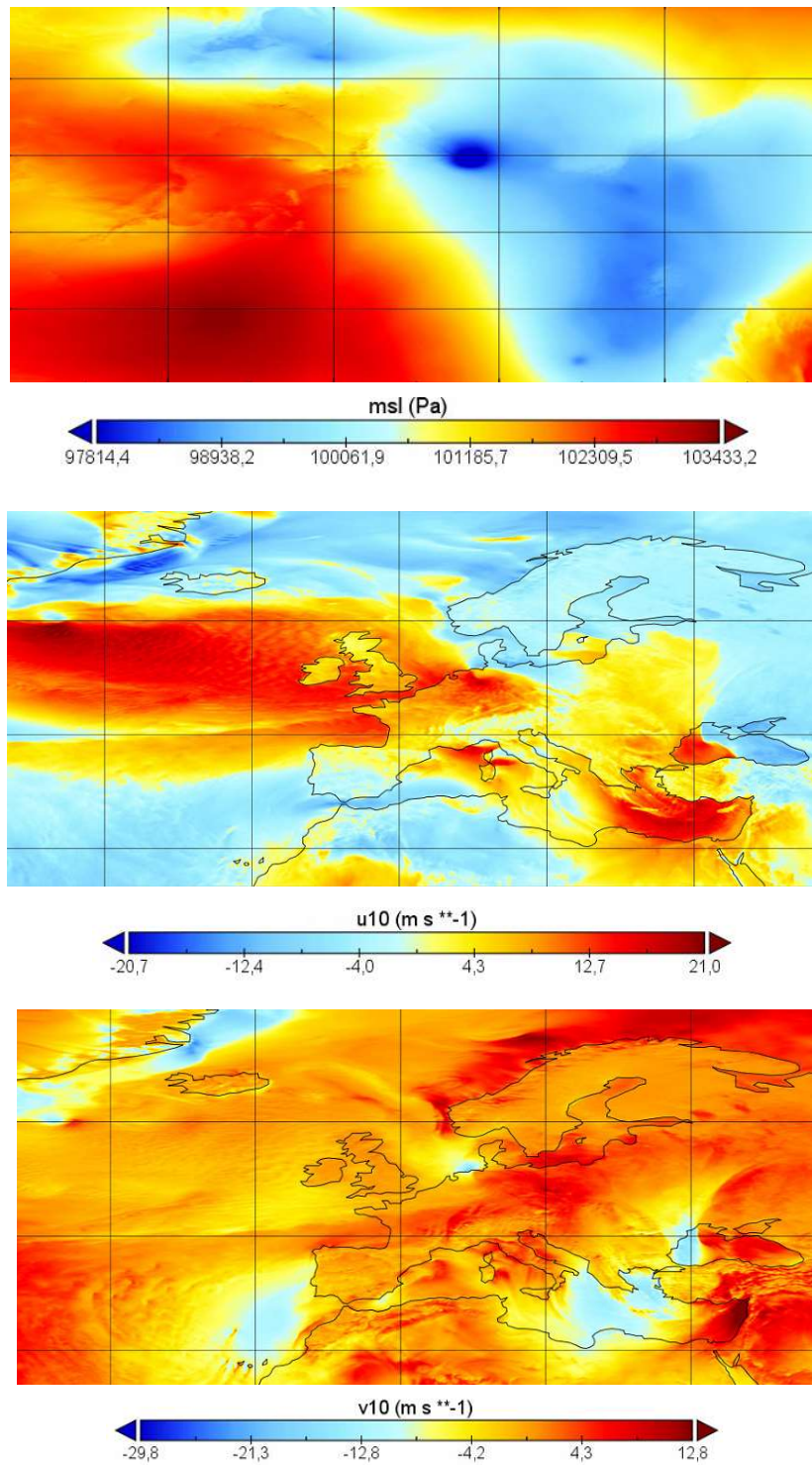


Figure A.3. The atmospheric pressure, eastward wind (u10) and northward wind (v10) of January Storm taken from JRC on January 18, 2018 at 12:00 UTC.

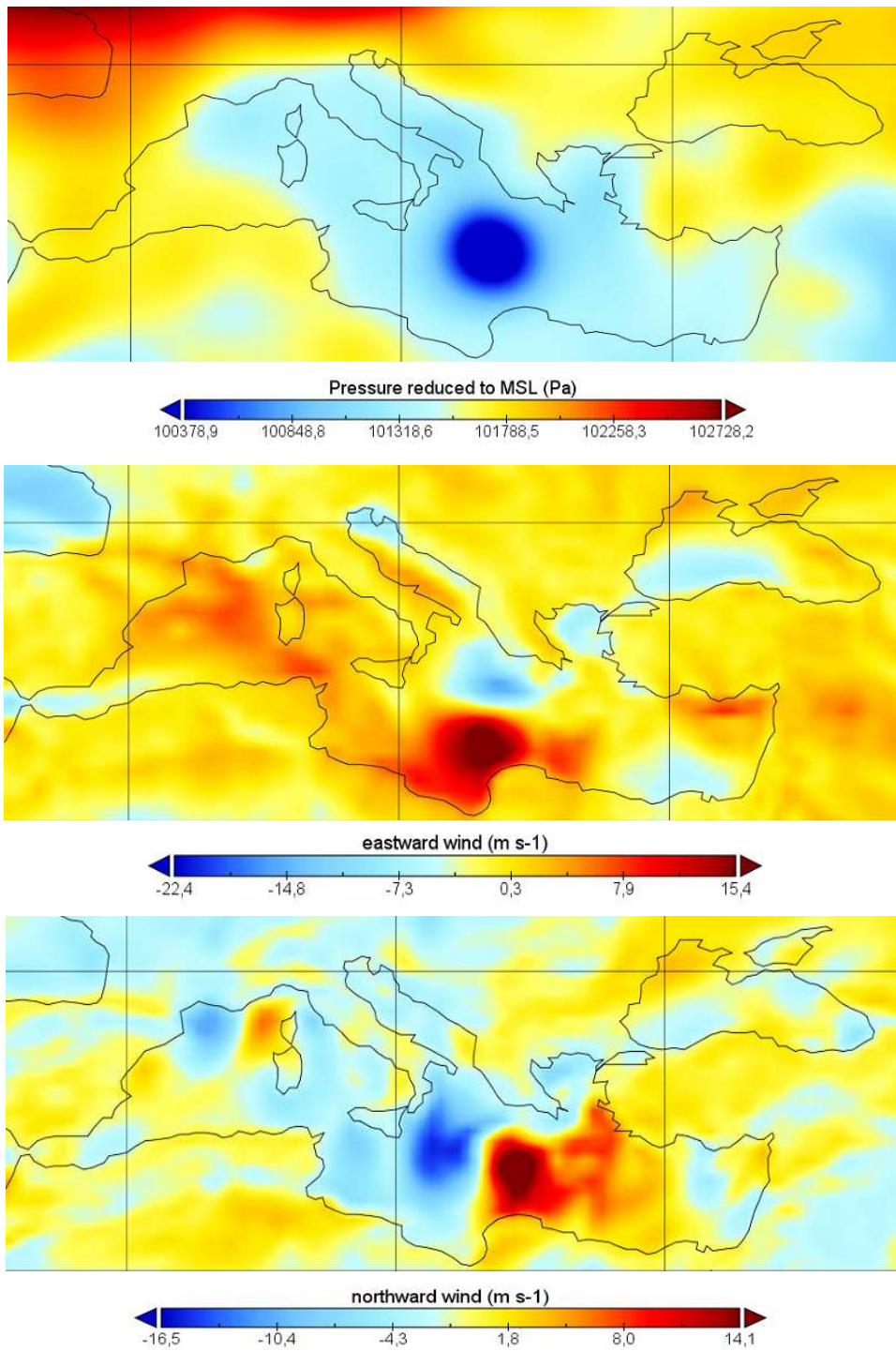


Figure A.4. The atmospheric pressure, eastward wind and northward wind data of January Storm taken from JRC on September 29, 2018 at 01:00 UTC.